Tampereen yliopisto

Aleksi Karjalainen

POWER SYSTEM FREQUENCY REGULATION WITH UPS RECTIFIER

Master of Science thesis
Information Technology and Communication Sciences
Examiner: Assist. Prof. Petros Karamanakos
Examiner: Prof. Sami Repo
March 2021

TIIVISTELMÄ

Aleksi Karjalainen: Sähkövoimajärjestelmän taajuussäätö UPS-laitteen tasasuuntaajalla
Diplomityö, 71 sivua
Tampereen yliopisto
Sähkötekniikan DI-tutkinto-ohjelma
Maaliskuu 2021

Nykyaikainen sähköjärjestelmä on jatkuvan muutoksen alla, sillä muun muassa ilmastonmuutoksen tuomat haasteet ovat pakottaneet meidät luomaan uudenlaisia ratkaisuja, jotta nykyinen teknologian kehitystaso voitaisiin ylläpitää ilman katastrofaalisia vaikutuksia maapallollemme. Sähkön tuotannossa tämä muutos näkyy lisääntyvänä uusiutuvien energiavarojen, kuten tuuli- ja aurinkovoiman, hyödyntämisenä. Näiden teknologioiden lisääntyessä, vakaan sähköjärjestelmän ylläpitoon tarvittavat keinot muuttuvat ja uusia haasteita voidaan havaita.

Yksi näistä haasteista on transienttitilanteissa havaittu taajuusstabiilisuus, jonka luomat ongelmat ovat yhä enemmän osa sähköjärjestelmää, kun uusiutuvat teknologiat korvaavat tavanomaisia sähköenergian tuotantomuotoja. Tämä johtuu siitä, että konventionaalisessa sähkön tuotannossa hyödynnetään isoja pyöriviä massoja, jotka tuovat inertiaa sähköjärjestelmään, mikä puolestaan parantaa stabiilisuutta esimerkiksi järjestelmän tehomuutoksissa. Uusiutuvat teknologiat sen sijaan ovat tyypillisesti kytketty verkkoon tehoelektroniikkaa hyödyntäen, mikä efektiivisesti erottaa niiden tuoman inertian verkosta. Tämän lisäksi, matalan inertian tuomat haasteet voidaan havaita erityisesti niin sanotuissa mikroverkoissa, joissa järjestelmä muodostuu pienemmistä tuotantoresursseista. Tyypillisesti nämä järjestelmät kykenevät saarekekäyttöön, jolloin kantaverkon tuoma inertia ja stabiilisuus häviävät. Tämän kaltaisissa matalan inertian järjestelmissä, taajuuden muutokset järjestelmän tehon muuttuessa ovat entistä isompia ja nopeampia, mikä voi aiheuttaa monenlaisia ongelmia verkkoon kytketyille laitteille.

Matalan inertian tuomia haasteita voidaan pyrkiä minimoimaan hyödyntämällä tehoelektroniikkaa sekä energiavarastoja. Erilaisten säätömetodien avulla, näillä laitteilla voidaan luoda ikään kuin virtuaalista inertiaa, ja täten parantaa järjestelmän taajuusstabiilisuutta. Tässä työssä tutkitaan keskeytymättömän virtasyöttöjärjestelmän (engl. Uninterruptible Power Supply, UPS) hyödyntämistä transientti taajuusstabiilisuuden parantamiseksi. Erityisesti työ keskittyy erittäin matalan inertian saarekekäytettävään mikroverkkoon, jossa sähkön syöttö saadaan diesel-varavoimageneraattorilta.

Työssä kehitetään säätöalgoritmi UPS-laitevalmistaja Eatonin 93PM 200 kW kolmivaiheiselle UPS-laitteelle, minkä tarkoituksena on säätää laitteen tulotehoa mitatun tulotaajuuden (ja taajuuden muutosnopeuden) mukaan. Kehitystyö tehdään aluksi simulaatioympäristössä vertaillen eri metodeja, minkä jälkeen kaksi säätömetodia (*linear droop and ROCOF-control*) implementoidaan oikeaan laitteeseen. Taajuussäätöä testataan sähkölaboratorioon rakennetussa saarekeverkossa, jossa UPS-laitetta syöttää dieselgeneraattori. Taajuussäädön suorituskykyä arvioidaan kytkemällä kuorma-askelia järjestelmälle ja mittaamalla taajuuden muutosta kuorma-askeleen aikana.

Taajuussäädön kehitys onnistui hyvin ja kuorma-askelien taajuuspoikkeamia saatiin kompensoitua erittäin tehokkaasti. UPS-laite oli selvästikin riittävän nopea vastaamaan rajuihin kuorma-askeliin, minkä ansiosta, esimerkiksi 160 kW kuorma-askeleessa, taajuuspoikkeamaa saatiin parannettua noin 8 Hz. Lisäksi UPS-laitteen taajuussäätö mahdollisti 200 kW kuorma-askeleen kytkemisen kerralla, mihin generaattori ei pystynyt ilman laitteen apua. Säätömetodeista lineaarinen droop toimi riittävän vakuuttavasti ja oli helpompi asetella toimimaan stabiilisti.

Avainsanat: UPS, taajuusstabiilisuus, inertia, virtuaalinen inertia, mikroverkko, generaattori, taajuussäätö, PLL, droop, taajuuden muutosnopeus, RoCoF

ABSTRACT

Aleksi Karjalainen: Power system frequency regulation with UPS rectifier
Master of Science thesis, 71 pages
Tampere University
Degree programme in Electrical Engineering
March 2021

The modern electrical power system is changing rapidly, as the global climate change forces us to implement new solutions, so that the present technological advancement can be maintained without catastrophic damage to the globe. In terms of power generation, this can be observed by the increasing amount of renewable energy sources, like wind and solar power. As the penetration of these technologies increases, the control of a power system changes, and new challenges are introduced.

One of these challenges is transient frequency stability, which is more evident as more and more renewables replace the conventional generation methods. This is because conventional generation utilizes large rotating masses that introduce inertia to the system, which in turn improves the stability. Renewable technologies on the other hand are grid-connected via power electronics and thus the inertia is decoupled from the system. Additionally, low inertia is also present in the so-called microgrid applications, where the system consists of small resources. Typically, these systems can operate in islanded mode, meaning that the stability and inertia of the utility grid is disconnected. In these systems, frequency deviations due to power imbalances are much faster and more severe, which may cause damage to grid-connected devices.

Power electronics and energy storage solutions can be utilized to mitigate the challenges that low inertia introduces. With proper control methods, these devices can be used to provide “virtual inertia” to the system, which enhances the stability. This thesis focuses on utilizing Uninterruptible Power Supplies (UPSs) to improve transient frequency stability, specifically in an extremely low-inertia islanded system, in which the generation is provided by a single diesel generating set.

A control algorithm for UPS manufacturer Eaton’s 93PM 200 kW three-phase UPS is developed that aims to control the device’s power based on the present input frequency (and rate of change of frequency). The development is first done in a simulation environment by comparing different control methods, after which two of the methods (*linear droop and ROCOF-control*) are implemented into a real device. The control is tested in a small-scale islanded system, where the UPS is fed by a diesel generating set. The performance is evaluated by analyzing the frequency deviations during load steps.

The simulation and the laboratory testing results showed that the developed control methods were successful, and the studied UPS device was able to compensate the applied load steps effectively. For example, the frequency nadir improved by approximately 8 Hz during a 160 kW load step with the linear droop and ROCOF-control methods. Additionally, the control methods enabled the system to survive a 200 kW load step without the generator tripping to underspeed. Both control methods showed promising results, but all in all the linear droop method was superior due to a more straightforward parametrization process.

Keywords: Uninterruptible power supply, UPS, frequency regulation, power system stability, microgrid, inertia, virtual inertia, generator, PLL, droop, RoCoF

PREFACE

This thesis was part of the Helios-project and was carried out at the Research and Development department in Eaton Power Quality Oy during February 2020 – March 2021.

I want to express my gratitude towards Eaton, and especially my supervisor Tuomo Kohtamäki, for giving me this excellent opportunity to learn and develop exciting technologies. Everyone at Eaton has been supportive during my efforts, even though at times it seemed that the time schedule just kept stretching. Additional thanks to Janne Paananen for his guidance and support.

The fact that I was able to do the testing using a real UPS device and a diesel generator really enhanced the thesis, and for that, I want to thank AGCO Power Oy for kindly providing us with the genset. Special thanks to Kari Mettälä and Jouko Järvinen for supporting in the genset-related stuff and showing interest in the thesis.

I would also like to thank my examiners, assist. Prof. Petros Karamanakos and Prof. Sami Repo for providing me with assistance and helpful comments.

Finally, I am grateful for the support and push I got from my friends, family and especially my girlfriend Anita, during the times my workload was immense.

Helsinki, 18th March 2021

Aleksi Karjalainen

TABLE OF CONTENTS

1. INTRODUCTION

The modern society is currently undergoing a critical period in terms of development of new technologies, especially in the energy sector. The evident implications of global climate change have transformed our way of thinking about energy production to a more sustainable way. The use of fossil fuel-based energy production has been decreasing and as a consequence of this development, the amount of renewable energy production is increasing [1]. Higher penetration of these technologies e.g., solar and wind power, will transform our power system in many ways. It will present new kinds of challenges as more and more of the conventional power generation units, large synchronous generators (SG), will be replaced by smaller, power electronics based distributed units. [2] [3]

The conventional synchronous generators are based on large rotating masses of which the kinetic (rotational) energy is converted into electrical energy. The combined amount of rotating mass in these generators can be observed as a total rotational inertia in the power system. Power system inertia can be defined as the opposing force that resists the impact of power imbalances on frequency changes. It is proportional to the stability of the system and the rate of change of frequency (ROCOF) in the event of transient changes, such as external disturbances, changes in load, etc. [2] [4] [5]

As the conventional synchronous generators are replaced by generators interfaced with power electronics, a decrease in power system inertia can be observed, as these technologies have limited (or no) inertia-factors [2]. In a low-inertia power system, a faulted generator or a sudden increase in the load could lead to an increased frequency deviation which may damage grid-connected equipment and even end in a complete collapse of the system. This kind of collapse situation is not a real concern in utility-scale grids since they still mainly consist of large generation units interconnected within vast areas and are dimensioned such that a loss of a single unit shall not lead to a collapse.

However, significant issues introduced by low inertia could be a problem in so-called microgrid applications [3]. A microgrid can be defined as a grid-connected entity that consists of an aggregation of small energy resources, energy storages and loads. A microgrid provides flexibility and controllability to the main grid via for example demand response services. Additionally, microgrids are typically designed to work autonomously

in islanded mode, which severely changes the nature of the power system. [6 – 8] When the microgrid transfers to islanded mode, the system is no longer benefitting from the stability of the main grid. The system inertia is now majorly decreased and mismatches between generation and consumption of electrical energy in the microgrid can be observed more evidently. Therefore, there is an apparent need for precise and fast control of the system to compensate for the lack of inertia.

One solution to maintain the power system stability and to contain the frequency is to introduce virtual inertia via power electronic devices and energy storages. Virtual inertia is a control method that transforms for example grid-connected energy storages into devices that emulate the inertia in synchronous generators by providing a similar response to power imbalances. This essentially can be seen as an increase in the power system inertia and thus the severity of frequency deviations can be mitigated. [3] [9]

As far as electrical storages and controllable power electronics are concerned, the uninterruptible power supply (UPS) has a lot of potential in this regard. Currently, Eaton EnergyAware UPS systems in data centers have shown to be capable of participating in primary frequency regulation using the energy from the batteries to add dynamical flexibility to the loading of the grid. [10 – 12] Additionally, Hansson conducted an initial study on the possibility of using UPS devices to provide virtual inertia and concluded that UPSs are well-suited for this kind of application [13].

The next step is to research the possibilities of these UPS systems to provide frequency support in islanded or isolated microgrids that could for example be a part of a data center facility. Figure 1-1 shows an example of this kind of microgrid with an UPS protected data center, renewable energy sources, battery storages and different types of loads. As the system is cut-off from the utility grid, the inertia derives mainly from the gas generating set (genset) and thus, the data center UPSs are used to provide frequency regulation to the microgrid, as well as their primary objective of protecting the data center.

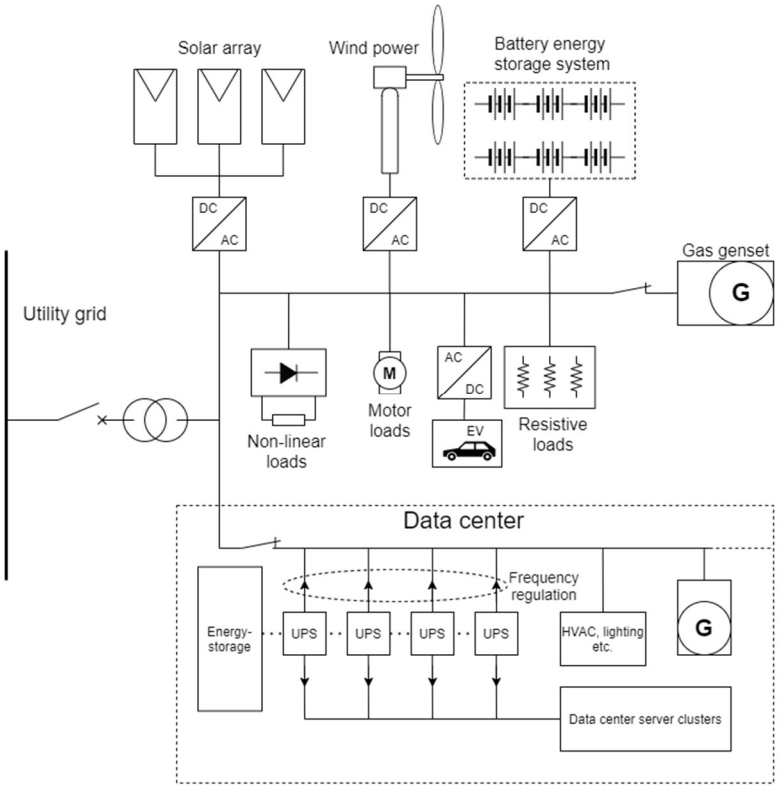

Figure 1-1: Example of an islanded microgrid with renewable energy sources, battery energy storage, back-up generator, different types of load and a data center equipped with UPSs providing frequency regulation to the grid.

1.1 Objective of the thesis

This thesis aims to study and develop a control method for UPSs that enables the devices to react to input voltage frequency deviations in the context of low inertia islanded or isolated microgrids. As the current Eaton EnergyAware UPS is intended for utility-scale grid frequency regulation, the control platform is relatively slow in the context of island/isolated systems. Thus, a faster control method is required. The goal is to achieve a fast enough response, that a power system with only a single diesel genset can be supported in large load steps and the frequency deviations are mitigated. The control method or algorithm is developed with the existing UPS control structure in mind and thus, it simply aims to calculate power commands for the UPS rectifier and charger based on the measured input frequency. The research question then is: is the studied UPS device (Eaton 93PM 200 kW) capable of providing fast enough power responses to mitigate the frequency deviations in the input? Different methods to calculate these power commands are considered and compared. As the control methods require fast tracking of the input frequency, the frequency measurement functionality of the UPS is improved as well.

The development of these controls is done in a simulation environment (MATLAB Simulink), where the performances are benchmarked by simulating load steps and evaluating the frequency deviations. In addition to the simulation work, the control system is verified by testing the operation in a small-scale islanded system constructed into a test laboratory. The developed control system is implemented for an Eaton 200 kW 93PM UPS device. A 250 kVA AGCO Power AG250 diesel generating set is utilized as the supply that feeds the UPS device and the resistive load banks in parallel. The performance is evaluated by applying similar load steps as in the simulations to the input-side of the UPS and measuring the voltages and currents which are later analyzed to gather frequency and power data. The control parameters are optimized in the process and different control modes and configurations are compared.

1.2 Structure of the thesis

First, in Chapter 2, a basic overview of double-conversion UPS devices and the relevant technologies and methods are given. This includes the UPS topology, the rectifier circuit, basics of the controls, grid-synchronization via phase-locked loop and some electrical energy storage considerations. The inverter or the output of the UPS device is not considered in this chapter, since it is not within the scope of this thesis.

Next, the theoretical background proceeds from power electronics to power system engineering and in Chapter 3, electrical grid stability is discussed. The chapter focuses on frequency stability and control in power systems and introduces essential matters such as power system inertia and frequency regulation. Virtual inertia methods and Eaton EnergyAware/UPS-as-a-Reserve (UPSaaR) features are also briefly discussed.

Chapter 4 focuses on developing the actual control system for the frequency regulation. This is done by extensive simulation work in MATLAB Simulink environment where a model of a diesel genset feeding a microgrid that consists of a resistive load bank and a UPS device is utilized. The performance of different regulation configurations is evaluated, and this is used as a guide for the implementation part of this thesis in Chapter 5.

In Chapter 5, a case study is conducted to verify the operation and performance of the developed control. A small-scale islanded power system with a diesel genset as the grid-forming unit is constructed, and measurements from load step tests are discussed and compared.

Lastly, in Chapter 6, the results and the entirety of the thesis is summarized, and some future research topics are discussed.

2. UNINTERRUPTIBLE POWER SUPPLY

There is an ever-rising need for continuous supply of electrical power, as the amount of electricity dependent technologies keeps increasing. Even though there are many investments made for improving the reliability of electricity transmission and distribution [14], there is still a need for technologies that keep the supply uninterrupted. These technologies are especially important for sensitive or critical loads such as data centers, medical facilities, and cell towers. Even a short voltage dip can cause significant losses to a manufacturing facility and damage the equipment. [15]

To maintain the reliability and the quality of the electricity supply, UPS systems are used. A stable voltage can be provided to the critical load, even in the case of an interruption of the utility grid. UPS systems need to respond quickly to the transient changes in the power system voltage, and supply power until the utility grid is restored to normal operation or until the back-up generators have started.

In this chapter, the double-conversion UPS is briefly introduced and some basic insight into the active rectifier technology used in the UPSs is provided. As for the controls of the rectifier, the grid synchronization via a phase-locked loop is discussed as this plays an integral part of the frequency regulation algorithm studied later in the thesis. Other components of the UPS, like the inverter are not included in the theoretical background as the focus of this thesis is on the input-side. Lastly, a brief introduction to different storage technologies used in UPS systems is given, so that the capabilities and limitations of UPSs in frequency regulation can be understood.

2.1 Double-conversion UPS

UPSs can be classified into static or rotary systems. Static UPS systems, which are the most frequently used, are purely based on power electronics (rectifiers and inverters) instead of motors and generators as in rotary systems. There is also a combination of the two, called a hybrid UPS system. [16] [17]

The basic functionality of a static UPS is that it rectifies the supplied alternating current (AC) to direct current (DC). The DC is used to charge the battery and thereafter, the DC is converted back to AC to the load through an inverter. When the supply is cut off by a fault, the battery starts discharging its energy and supplying the load through the inverter. [16] Static UPS systems can be divided into three different topology/configuration types: online, offline, and line interactive UPS. Each of these have the same above-mentioned functionality but differ slightly in the operation and performance. [17] [18] The topologies are the very basic configurations of UPS systems and there is a multitude of different variations based on these.

Online UPS, also as known as double-conversion UPS or inverter-preferred UPS, basic topology is shown in Figure 2-1. A distinctive feature of the online UPS is that the electrical power from the connected AC system is continuously supplied through the rectifier to the DC bus, where a steady DC link voltage is maintained. This means that the rectifier needs to be fully rated for the protected load and the charging of the battery. As can be seen from the block diagram in Figure 2-1, the inverter is connected in series with the protected load. With this configuration, a seamless transition from normal mode to battery supplied mode can be made. The battery is typically interfaced with a charger circuit to control the charging current and add protection. A static bypass switch is also typically included in these systems to introduce redundancy of the supply. The switch can be used to bypass the whole converter configuration in the event of malfunction, overload, or maintenance without interrupting the supply of the protected load. [17 – 21]

The two previously mentioned alternative static UPS topologies, offline and line interactive UPS supply their output load without the back-to-back conversion and thus are not capable of seamlessly transferring to battery mode. Most of the high-power UPS systems and the UPSs studied in this thesis use the double-conversion topology, and thus no further description of other topologies is discussed here. In [18], a comprehensive review of different topology and circuit configurations of UPSs is presented. These topologies include transformers, additional power electronics converters and different switch configurations. A lot of customization can be made to the UPS systems depending on the

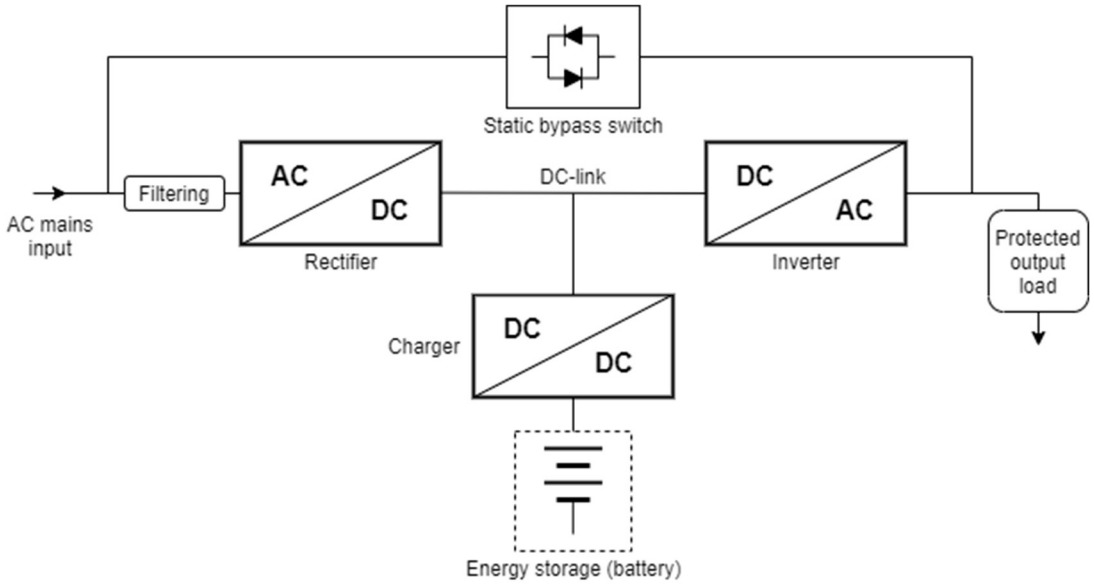

Figure 2-1: Typical double-conversion or online UPS topology block diagram.

application and requirements. Selecting the right topology and type of UPS system is a sophisticated problem which requires exact knowledge about the application and requirements in order to make the trade-off between different specifications and features optimized.

The system level topology in for example a data center UPS system depends on the desired level of redundancy and protection. To ensure high uptime and reliability, the UPS systems are over dimensioned in terms of normal operation. N, N+1, 2N and 2N+1 topologies shown in Figure 2-2 are the most common. The N topology has no redundancy as the UPS capacity (3 x 1 MW) is exactly the rated load amount (3 MW). N+1 topology on the other hand provides an additional redundant UPS to the system, and thus a single unit failure can be tolerated. Moreover, 2N topology provides even more redundancy with a completely independent secondary power path that can supply the rated load. Lastly, the 2N+1 topology adds a redundant UPS to both power paths. [10] [15]

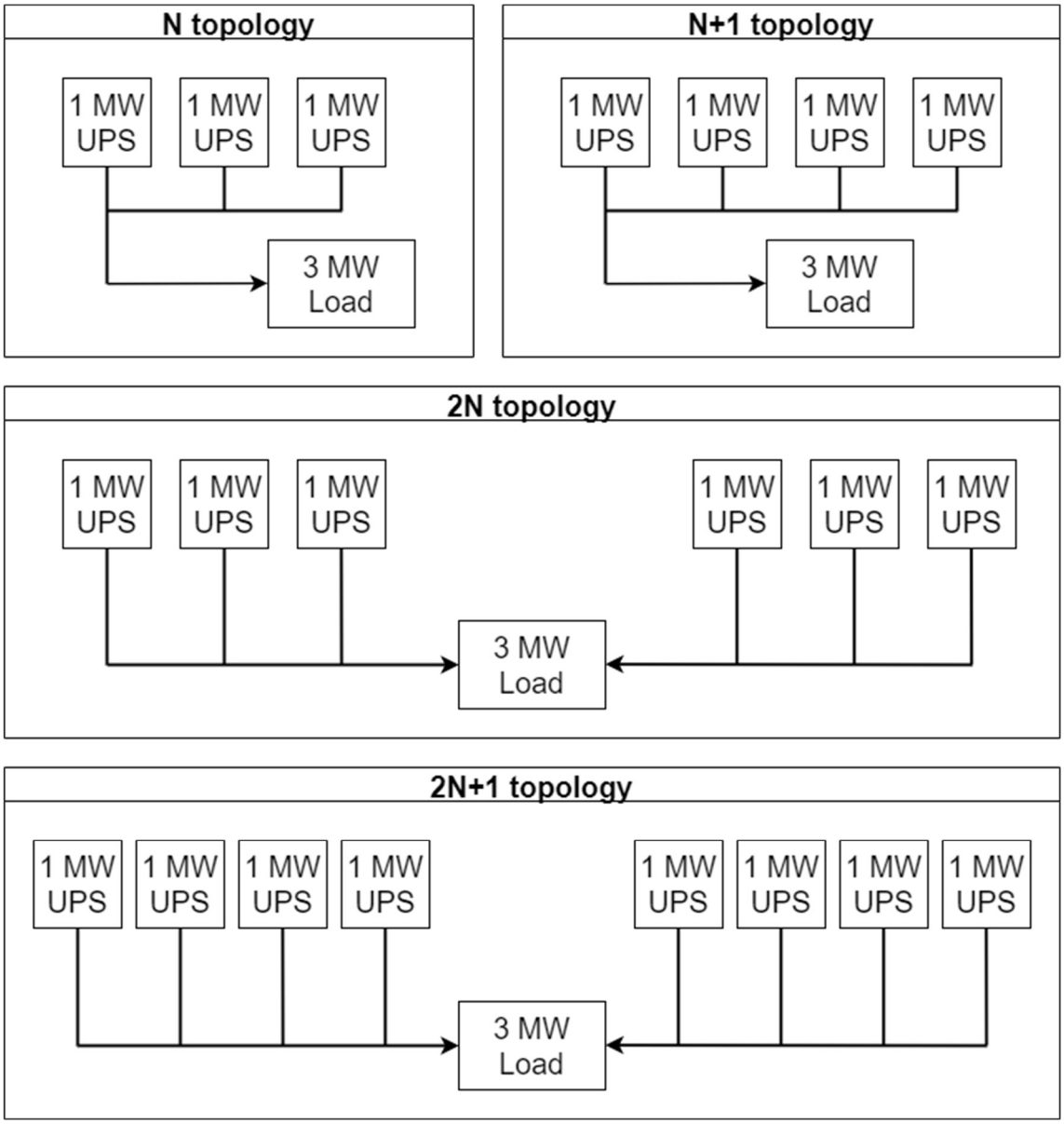

Figure 2-2: Typical system-level UPS topologies to provide redundancy.

2.2 UPS active rectifier

A crucial component in the operation of a UPS device is the rectifier that is used to convert the AC mains supply to DC voltage, and which in turn is used to charge the battery by a charger. This is also the technology that enables the frequency regulation scheme that is described in Chapter 4, and thus it is now briefly introduced. However, as the focus of this thesis is not on the design and control of the rectifier and/or battery charger, the matter is discussed more generally to describe the platform that the frequency control is used on. Additionally, as the thesis only extends to dealing with the input-side of the UPS, no further introduction to the inverter/output-side is given.

In state-of-the-art UPS systems, the rectifier is based on insulated gate bipolar transistors (IGBTs) that act as voltage-controlled switches [22]. A rectifier which utilizes IGBTs instead of for example diodes, can also be called an active front end (AFE) or an active rectifier. The converter is connected to the supplying grid through a passive filter, usually an inductor, or capacitor and inductor combination, to ensure lower harmonic disturbances and noise caused by the inherent switching actions in the converter. Power quality issues such as harmonics are a very crucial part of the UPS input-side design because the AC to DC conversion affects the feeding grid, as the devices are grid-connected. [21] [23] [24] Different standards and requirements set by e.g. the customer need to be complied with. For example, the IEC 61000-3 standard specifies limits for total harmonic current emissions and the IEC 62040-3 sets performance and test requirements for UPSs specifically [25] [26]. This is mostly why, even though more expensive, active rectification has replaced passive rectification with e.g., diode rectifiers in most of the applications. By utilizing active rectification topologies, the input current waveform can be made close to sinusoidal even in partial, unbalanced, or non-linear loading operation. [24]

As in most power electronic equipment, there exists multiple different topologies, configurations, and control methods for rectifiers. Depending on the DC link voltage level, the energy storing component and the switch type, active rectifier topologies can be split to voltage source rectifiers (VSR) and current source rectifiers (CSR) [24]. In the scope of this thesis and in the context of the UPS systems studied in this work, the so-called three-phase three-level neutral point clamped (NPC) converter topology is considered. Additionally, the rectifier can be classified as a VSR, due to the boosted DC link voltage, bidirectional switching arrangement and DC link capacitor elements.

An NPC converter, shown in Figure 2-3, consists of four switching modules, split into positive and negative rails, and two clamping diodes, per each phase. Each of the input

phases on the AC side are connected to their own converter leg. The switching modules in the legs consist of a transistor (e.g. IGBT for low voltage applications) and an anti-parallel diode. In the DC link of the converter, two DC capacitors, C1 and C2, are connected to the neutral point (o) of the system. The voltages of the capacitors, V_{c1} and V_{c2}, make up the net DC link voltage $V_{dc} = V_{c1} + V_{c2}$. The purpose of the diodes is to clamp the voltage in the switching modules so that the voltage across the module is the same as in one of the capacitors, i.e. $\frac{V_{dc}}{2} = V_{c1} = V_{c2}$ in a balanced situation. The three-level NPC is a multi-level converter, which have gained a lot of popularity for example due to their low THD input current and reduced voltage stresses on the switching modules. The three levels refer to the possible phase voltage levels, with respect to the neutral point potential, generated by the switching actions of the converter: $\pm\frac{V_{dc}}{2}$ and 0. [21] [27] [28]

Due to the bidirectionality and controllability of the IGBT switch configuration, the active rectifier can handle reverse power flow i.e., it can be used as an inverter. The IGBT itself cannot conduct in the reverse direction, but the anti-parallel-connected freewheeling diode is used for this purpose. [24] This way, when the load side of the system has excess energy, it can be supplied back to the grid without letting the DC link voltage rise over the rated limit of the DC link capacitors. As for the rectifiers used in UPS devices, the bidirectionality of the system can be utilized to feed energy from the energy storage back to the grid when needed. This feature is the main enabler of the technology that is being studied in this thesis.

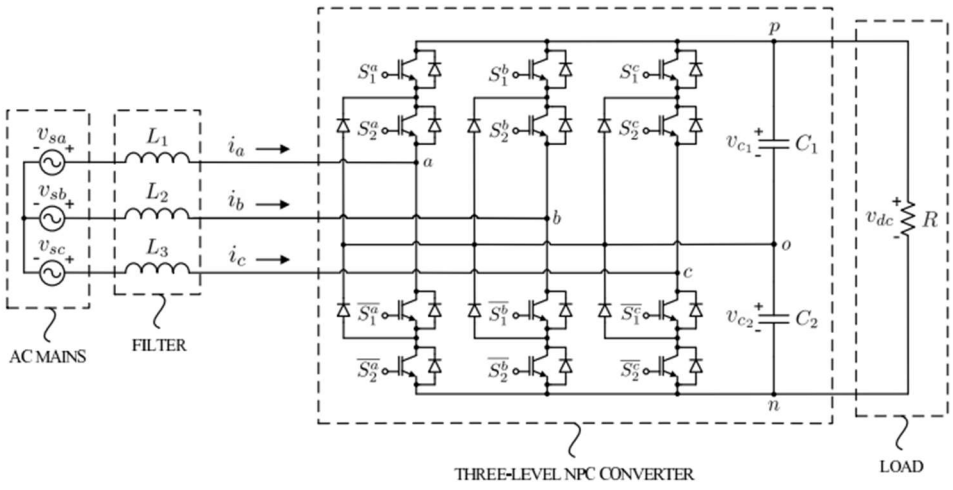

Figure 2-3: A three-phase three-level neutral point clamped converter. [29]

The control system for the rectifier usually consists of multiple control loops and may be implemented in various ways, but the aim is to achieve regulated and stable DC link voltage and minimize the input current THD. Generally, the DC link voltage control is a feedback loop that ensures that the DC link voltage is kept at the reference value by controlling the power drawn from the input. The reference value for the DC link voltage needs to be set higher than the peak voltage in the clamping diodes to prevent passive rectification through the diodes. In addition to controlling the DC link voltage amplitude, the DC offset, or the neutral point potential, must also be controlled. The DC link voltage control forms a reference for the inner loop that controls the rectifier current. Here, different control techniques such as vector control, instantaneous active and reactive power control and power factor correction can be implemented. Regardless of the control technique, the switching of the transistors is then controlled by pulse width modulation (PWM), which can also be implemented in various ways. [18] [23] [29] In the context of UPS applications, the rectifier also needs to work in unison with the battery charger component. Additionally, the control system generally includes protective functions, for example a current limit for the rectifier to prevent overloading the components.

2.3 Grid synchronization and phase-locked-loop

When dealing with devices connected to the grid, it is essential that the state of the grid is somehow monitored, and this can be challenging when the grid is dynamic in its nature. The load and the generation capacity of the grid is constantly changing and nonlinearities are present. In three-phase systems, the voltages are not independent of each other, rather they should be considered as a vector that consists of three voltage components. In normal conditions, the voltage components have constant and equal frequency, amplitude and relative phase shifting. However, this is not always the case since disturbances in the grid produce unwanted changes in the voltage vector, which could lead to damaged equipment or increased power losses. Therefore, these non-idealities should be considered when designing the controller for a grid connected converter, since they are especially sensitive to distorted voltages.

To gather information about the fundamental component of the feeding grid and achieve synchronous operation, grid synchronization is used. Grid synchronization can be done with an open- or a closed loop system, but zero crossing detection -based open loop systems tend to be slow and very sensitive to frequency noise, voltage distortions and imbalances [30] [31]. Closed loop grid synchronization is done with a phase-locked loop (PLL) which is a feedback control system that yields much more precise results. The

basic function of a conventional PLL is that the generated phase of the voltages is matched with the grid input phase. [31] [32]

For proper and accurate grid synchronization, the system needs to reject high-order harmonics and be capable of tracking the voltage even in transients. Most popularly, three-phase grid synchronization is realized by utilizing the synchronous reference frame-based phase-locked loop (SRF-PLL or dq-PLL). The SRF-PLL converts the three-phase voltages *a, b* and *c* into two components, *d* and *q*, in rotating reference frame with the so-called Park's transformation. The transformation to SRF can be mathematically presented as:

$$\begin{bmatrix} v_d \\ v_q \end{bmatrix} = \frac{2}{3} \begin{bmatrix} \cos(\theta') & \cos(\theta' - \frac{2\pi}{3}) & \cos(\theta' + \frac{2\pi}{3}) \\ -\sin(\theta') & -\sin(\theta' - \frac{2\pi}{3}) & -\sin(\theta' - \frac{2\pi}{3}) \end{bmatrix} \begin{bmatrix} v_a \\ v_b \\ v_c \end{bmatrix} \quad (2\text{-}1)$$

where v_d and v_q are the voltage *d* and *q* components, respectively, and θ' is the grid voltage phase angle. The rotation of the reference frame is PI-controlled (proportional-integral) via a feedback loop such that the q-component is regulated to zero. The additional scaling factor of 2/3 is used in the reference frame transformation in Equation (2-1) so that the actual amplitude of the input voltage vector remains the same in both reference frames. This results in the d-component representing the amplitude of the voltage and the phase angle information is given by the output of the feedback loop, as seen from the block diagram in Figure 2-4. [31] [32]

Tuning the SRF-PLL is a trade-off between speed and accuracy: with healthy input voltages, a high bandwidth will yield a fast and accurate response, and even in the case of voltages polluted by high-order harmonics, a reduction in the bandwidth and the use of a filter will be enough to obtain good results. However, with unbalanced input voltages, tuning of the PLL bandwidth is not an adequate measure to yield accurate results. This is due to a mismatch between the positive sequence component[1] and the voltage d-component which is the result of frequency oscillations in the grid [32] [1]. A more precise grid synchronization method under unbalanced three-phase voltages is to use the decoupled double synchronous reference frame PLL (DDSRF-PLL). It utilizes two separate reference frames for positive and negative synchronous speeds and a decoupling network to cancel out oscillations. [31] In addition to this, there are several different PLL

[1] Positive sequence component is a representation of the three-phase voltage from a symmetrical component transformation. The phase sequence is the same as in the original voltage signal.

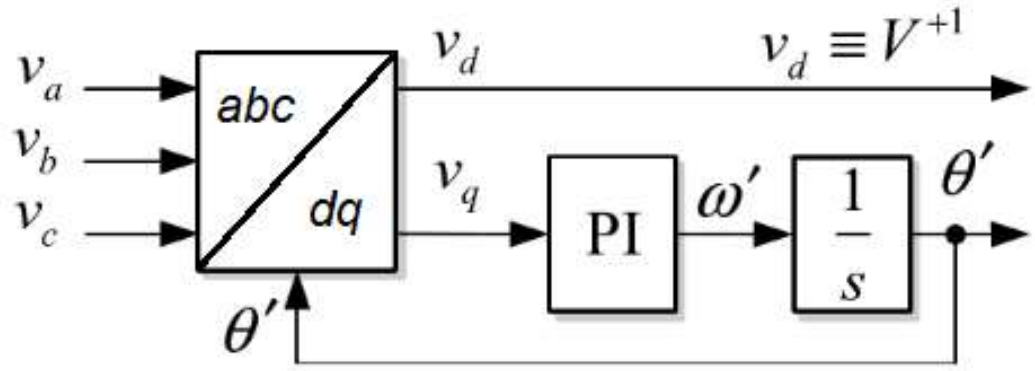

Figure 2-4: SRF-PLL block diagram. [31]

topologies with unique characteristics suited for different types of applications. Reviews of different PLL topologies can be found from [32 – 38].

The conventional method for line frequency calculations from a digital PLL structure derives from the phase information θ' which is the result of integrating the angular frequency ω' as shown in Figure 2-4. The frequency is then calculated based on the sampling frequency of the digital controller and a counter which keeps track of the inner controller loop during a line cycle. The accuracy of this type of frequency calculation is limited by the sampling frequency of the digital controller since the incremental phase changes are proportional to the sampling time. In [39], a direct frequency measurement based on the angular frequency ω' is proposed. The working principle in the proposed method is that the angular frequency is summed up during a line cycle and after the line cycle ends, the averaged frequency can be calculated by dividing the summed angular frequency with a counter variable. The paper suggests that the proposed method is 80 times more accurate in terms of frequency measurement error than the conventional method.

However, both described frequency measurement techniques sample the frequency data every line cycle i.e., for 50 Hz system, the frequency is sampled every 20 ms. This kind of performance is acceptable in a utility-scale grid as will be discussed later in Chapter 3. In the implementation part of this thesis, the aim for the PLL is to achieve fast dynamic response so that the rapidly changing frequency of the feeding grid can be used as a control input for the frequency regulation algorithm. As will be demonstrated later in the thesis, the line cycle –based frequency measurement sampling may not be fast enough. Additionally, the frequency measurement cannot be too noisy, so that the control system remains robust, and stable steady-state operation is maintained. The use of filtering techniques to suppress the impact of harmonics and noise causes even more delays to the frequency measurement. These delays will limit the capability of the designed frequency regulation control system and need to be considered [40].

In the scope of this thesis, the presence of harmonics, unbalanced voltages and other abnormalities are not fully considered in the performance of the PLL/frequency measurement, thus a simple SRF-PLL can be utilized. The implementation of the frequency measurement will be discussed more in detail in Chapter 4.

2.4 UPS storage technologies

When the AC mains supply falls out of the desired tolerance or gets interrupted, the UPS starts feeding electrical energy to the protected load from the energy storage of the system. The energy storage of the UPS can be for example a battery or a flywheel. In addition to this, supercapacitors are an alternative storage technology that has a lot of useful qualities in UPS applications. The fundamental properties of electrical energy storages from which a review of their capabilities can be done include, but are not limited to:

- Capacity (kWh) and energy density (Wh/kg),
- Charge/Discharge power (kW),
- Efficiency (%),
- Cyclability and ageing,
- Response time, i.e., the time it takes to start discharging the battery (s),
- Operational temperature range,
- C-rate, which is a measure of discharge speed,
- Depth-of-Discharge (DOD), and
- Cost

In this subsection, a basic overview of the two most common battery technologies, valve-regulated lead-acid (VRLA) and Lithium-ion (Li-on), is conducted. The benefits of using supercapacitors are also reviewed.

VRLA

In high power applications, lead-acid batteries are the most economical solution and they have been under extensive research and development for over 100 years, making them a reliable choice for UPS systems. However, lead-acid batteries suffer from a process called sulfation, in which lead-sulfate crystals build up on the electrodes of the battery and decrease the capacity. Lead-acid batteries should not be discharged too deeply since this increases sulfation. [41] In addition, VRLA batteries benefit from strict thermal control since the appropriate operational temperature is 20 – 25 °C. Higher temperatures

will shorten the service life and lower temperatures will decrease the battery capacity. The short cyclic life of the VRLA does not propose a problem in UPS applications, since the amount of charge/discharge processes is relatively low, and most of the time the batteries are fully charged. Lead-acid batteries are also heavier compared to other battery chemistries and the charging process is relatively slow. [42 – 44]

Li-ion

For improved cyclic characteristics and larger energy density, Li-ion batteries are a promising technology that have sparked a lot of interest in the recent years. Li-ion is still initially more expensive than lead-acid technologies, but the price has come down and is predicted to continue decreasing. The initial cost of using a Li-ion battery can also be justified due to their longer service lifetime and lower costs regarding the operation and maintenance. Because of the high energy density of the Li-ion battery (~2.5 times higher than VRLA), they are commonly used in portable applications for example mobile phones. Li-ion batteries also have better discharge efficiency, and higher power charging is tolerated. These properties, being able to keep the Li-ion battery partially charged and the cyclability makes it a good candidate for demand response services. [42 – 44] A comparative review between Li-ion and VRLA batteries is made in [42], where over 40 different technical specifications are compared.

Supercapacitors

As an alternative to electrochemical batteries, supercapacitors are a potential electrical energy storage solution for UPS systems. A comparison between some characteristics of a typical supercapacitor and a battery is shown in Table 2-1. As the properties in the table indicate, supercapacitors have better peak power capabilities and power density. Additionally, cyclic characteristics and response times are far superior. On the other hand, supercapacitors have poor energy density (around 1 – 10 Wh/kg as opposed to 20 – 100 Wh/kg in chemical batteries) and thus a longer duration storage is not possible [43]. For example, the supercapacitor strings that are utilized in Eaton UPS systems can provide around 10 seconds of back-up time at 100 kW [45].

One possibility for UPS systems is to implement a hybrid storage system, where a supercapacitor is used for the initial power demand and a battery pack provides extended supply during longer outages [18]. This kind of solution is used in the Eaton UPSG-shipping container system, which consists of a generator and UPS system with supercapacitors as a storage [46]. As will be briefly discussed in Chapter 6, supercapacitors could

also be suited for fast frequency regulation purposes in low-inertia grids, as only a short burst of power is required.

Table 2-1: Typical characteristics of a supercapacitor and a battery. [43]

	Supercapacitor	**Battery**
Discharge time	1 – 30 s	0.3 – 3 h
Charge time	1 – 30 s	1 – 5 h
Cycle life	>500 000 cycles	500 – 2000 cycles
Efficiency	90 – 95 %	70 – 85 %
Power density	1000 – 2000 W/kg	50 – 200 W/kg
Energy density	1 – 10 Wh/kg	20 – 100 Wh/kg
Operating temp.	-40 – 70 °C	0 – 60 °C

3. ELECTRICAL GRID STABILITY

The main function of an electrical power system is to provide electrical energy for the whole system reliably, and at the same time, keep the quality of the supplied power at applicable limits. The power system needs to maintain constant frequency and voltage, even in the event of sudden changes in loading or generation. The electrical grid is subjected to continuously changing environment and when a transient disturbance occurs, the reaction of the system is dependent on the type and magnitude of the disturbance as well as the initial condition. [47] [48] The power system's ability to recover from transient disturbances is defined as *power system stability*. It describes the system's reaction to a physical disturbance and how it can continue stable operation afterwards. For a power system to be stable, all the generators and loads that are not directly subjected to the fault need to continue operation without tripping and maintain supporting the grid. Conversely, an unstable power system will not reach a state of equilibrium, and a major fault could lead to a complete collapse of the system. [49]

Power system stability can be considered as a unified description of the system's performance. However, it is more practical to analyze stability in different categories and classifications since there is a lot of different influencing factors that may yield instability in the system. The type of disturbance divides the classification of the system stability into two: small-signal stability and transient stability. Small-signal stability addresses the system's reaction to small variations in e.g., loading and generation. Transient stability on the other hand deals with larger disturbances that affect the system parameters in a much larger scale. The transient stability of the system may differ heavily depending on the origin of these disturbances (loss of generation or loading, faulted interconnections etc.). This means that for a complete analysis of a power system's transient stability, a thorough investigation of different scenarios regarding disturbances and initial conditions should be conducted. [48 – 50]

Another way of categorizing power system stability is by considering the variations in different system parameters that indicate instability. This results in three different categories in which transient and small-signal stability can be analyzed: rotor-angle stability, frequency stability and voltage stability. Rotor-angle stability focuses on interconnected synchronous machines and how they can continue synchronous operation following a disturbance in the system. Voltage and frequency stability describe the system's ability

to maintain steady voltages and frequency, respectively, throughout the whole system after being subjected to a disturbance. [48 – 50]

In the scope of this thesis, the focus is on transient frequency stability and how a power system reacts to sudden imbalances between generation and load. The response to imbalances is directly related to the inertia of the power system and thus, the basic concepts regarding inertia and synchronous generators are discussed in this chapter. Power system frequency regulation and frequency standards are introduced, and the concept of virtual inertia and current state of energy storage utilization in power system frequency regulation is also presented. Even though the simulation and implementation part of this thesis is about extremely low-inertia islanded/isolated microgrids, the following background theory includes discussion about utility-scale power systems so that some reference can be established.

3.1 Power system inertia and synchronous generators

As stated in the introduction of this chapter, power system frequency is one of the parameters that should be maintained at a specified value or at least within a desired range. In electrical power systems there are three different factors that attribute to the deviation of frequency: power imbalance, inertia, and reserves. Power system inertia can be defined as the opposing force that resists the impact of power imbalance on frequency changes. This opposing force is caused by the kinetic energy stored in the rotating masses in the generators connected to the power system. [4] [5]

In current electrical grids, the main source of electrical energy is provided by synchronous generators. As the name suggests, these machines require to be in synchronous operation, meaning that the average electrical speed of the generators needs to be maintained at constant throughout the whole interconnected system. In steady-state operation, a balance between mechanical input power and electrical output power is maintained and respective torques are produced. The direction of mechanical and electrical torques are opposite to each other, the mechanical torque direction being in the direction of rotation. [5] [47] [48]

When an interconnected system with synchronous generators is faulted or a power imbalance occurs, a difference in the mechanical and electrical torques of the machines can be observed. This torque difference leads to an increase or a decrease of the rotor speed and if the speed deviates enough, the protection system will isolate the generator from the system leading to another disturbance (loss of generation) observed by the

other generators. However, generally power systems are dimensioned in a way that a single disturbance should not lead to cascading faults. The variation of the speed and the relationship to the torque difference can be expressed with the so-called swing equation as

$$\frac{2H}{\omega_n}\frac{d^2\delta}{dt^2} = T_m - T_e \qquad (3\text{-}1)$$

where ω_n is nominal angular speed of the rotor [rad/s], δ is the rotor angle [rad] and T_m and T_e are the mechanical and electrical torques of the machine, respectively. A defining parameter for synchronous generators and their stability is the inertia factor or inertia constant *H*, which describes the amount of kinetic energy stored in the machine. It is essentially the time in seconds, that the generator would need to operate with nominal power to output the equivalent amount of energy. Inertia constant of a machine can be expressed as

$$H = \frac{1}{2}\frac{J\omega_n^2}{S_n}\ [\mathrm{s}] \qquad (3\text{-}2)$$

where *J* is the inertia of the machine [kgm^2] and S_n is the nominal apparent power of the machine [MVA]. [5] As described before, and as can be seen from the swing equation, the synchronous machine accelerates/decelerates when there is a torque mismatch, and the accelerating torque can be expressed as

$$T_a = J\frac{d\omega}{dt}. \qquad (3\text{-}3)$$

By combining Equations (3-2) and (3-3), the accelerating power P_a can be extracted as

$$P_a = T_a\omega_n = \frac{2HS_n}{\omega_n}\cdot\frac{d\omega}{dt}. \qquad (3\text{-}4)$$

Equation (3-4) can be solved for the ROCOF [Hz/s], i.e., the derivative of the system frequency by replacing the angular speed [rad/s] with frequency *f* [Hz]:

$$\frac{df}{dt} = \frac{P_a f_n}{2HS_N}. \qquad (3\text{-}5)$$

With this equation, the initial ROCOF of the system can be determined, if the power imbalance i.e., loss of generation or addition of load is known, since

$$P_a = \mathrm{P_{gen}} - P_{load}, \qquad (3\text{-}6)$$

where P_{gen} and P_{load} are the generation and connected load of the system, respectively. From these equations, it can be deduced that higher inertia constant *H* decreases the ROCOF of the system after a power imbalance event. The importance of inertia in a power system is illustrated in Figure 3-1, where different frequency responses for different system inertias are represented. The blue and green lines with system inertia around 3.5 show the highest initial ROCOF and the frequency nadir (minimum) is the lowest. As the inertia is increased, the response improves in terms of decreased initial ROCOF and increased nadir. The figure also shows that the recovery period after the nadir is slower as the inertia is increased, and thus the settling time of the frequencies are similar.

The inertia constant can also be defined for the whole system by combining all the grid-connected machine inertia constants:

$$H_{sys} = \frac{\sum H_i S_i}{\sum S_i}. \qquad (3\text{-}7)$$

It should be noted that also some loads have inertia, and they should be included in the system inertia constant H_{sys}, since they affect the stability of the system in the same way as generators. Furthermore, the frequency response of a system is expressed by the swing equation for only the initial transient period (inertial response). After that, the frequency of the system is affected by the control actions of the generators and inertia is not the only defining parameter regarding frequency. Currently, and in the future, as more

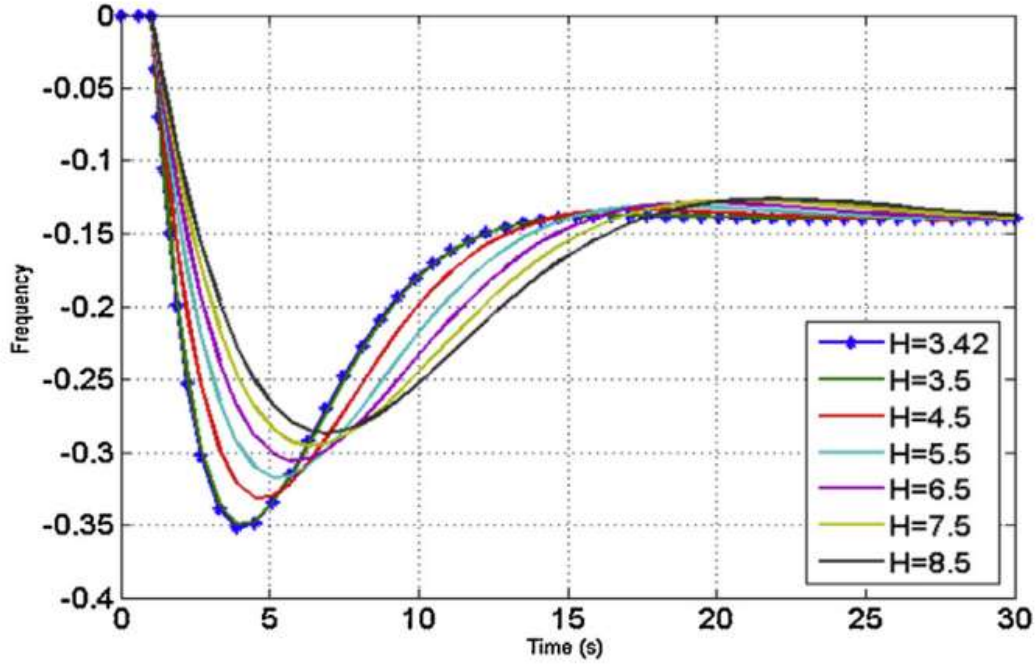

Figure 3-1: Frequency response of a power system with different system inertias. Y-axis represents the frequency deviation from the nominal, in Hz. [51]

and more large SGs are replaced by renewable energy sources, the overall power system inertia decreases. This is because technologies such as wind turbines and solar arrays are connected to the grid through power electronic converters which effectively decouples the energy source from the grid and thus, no inertia is added. [4]

3.2 Frequency regulation and control

Primary frequency control in generators is done by controlling the active power output, which in turn is controlled by the prime mover and its mechanical power output. Whether the prime mover is a steam/gas turbine or a diesel engine, the mechanical output power is regulated by controlling the input of the source of energy. For example, in steam turbines, the input steam is regulated by opening and closing the valves that let the steam flow into the turbine. A basic block diagram of a synchronous generator's frequency control is shown in Figure 3-2. The figure shows that a supplementary frequency control loop is also usually added into larger synchronous generators, which provides additional restorative capabilities by adjusting the load reference setpoint. The speed of the machine is controlled by the speed governor, which controls the system by considering the power command from the supplementary control loop and the change in rotor speed. [50] It should be noted that in practical utility scale grids, especially in Europe, frequency regulation is not this simple, as most of the generators are used to provide constant power, and only some of them will participate in frequency regulation. These market-based services are discussed in the next subsection.

The synchronous generators output power is controlled by the so-called speed governor, that can be controlled in *droop* or *isochronous mode*. The difference between these two modes is that the established frequency of generator output is fixed in isochronous mode but varied in droop mode. In droop mode, the frequency changes as a function of the

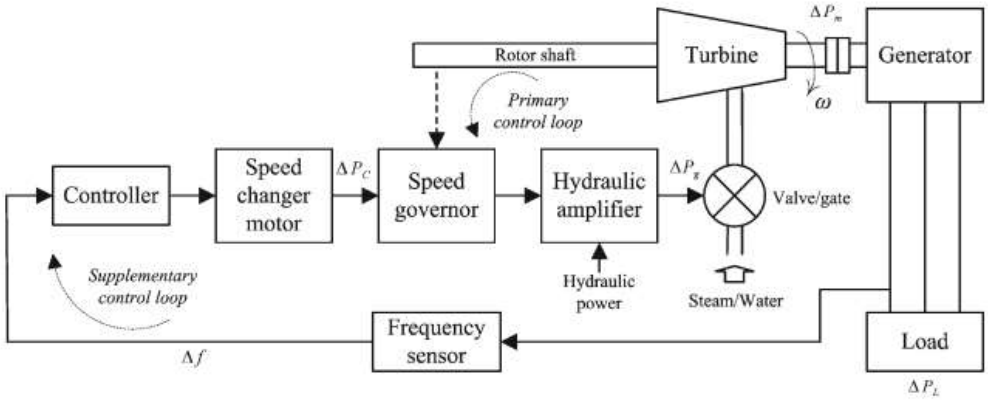

Figure 3-2: Block diagram of a synchronous generator's frequency control loops. [50]

load level in the system, which enables load sharing among parallel generators. The output of the generator is inversely proportional to the frequency, for example, when the droop setting of the generator is 5 %, the generator will output 100 % of its power when the frequency has decreased by 5 %. This is essentially useful in power systems with multiple generators and highly variable loading situations but will cause steady-state frequency error in situations where the loading is off nominal. [52] Therefore, a supplementary control loop, as shown in Figure 3-2, is required. Figure 3-3 shows an example of speed-droop characteristics in a 50 Hz grid with 4 % droop setting. In a power system where the frequency is maintained at a constant, when the speed-droop curve of the generator is changed from the lower (orange) to the upper (blue), the generator will pick up more power. For example, at 50 Hz the lower droop setting corresponds to 75 % of load power and the upper setting is at 100 %.

In isochronous mode, the speed of the generator is constant, and frequency is maintained at nominal regardless of the loading level. This is done by rapidly regulating the energy input to the prime mover when the loading changes. Isochronous mode control can be used when the generator is either the only generator supplying the system or the largest unit, but problems arise when multiple generators are controlled isochronously in parallel. Parallel operation would require communication between the generators which becomes challenging and expensive when the number of generators increase. [50]

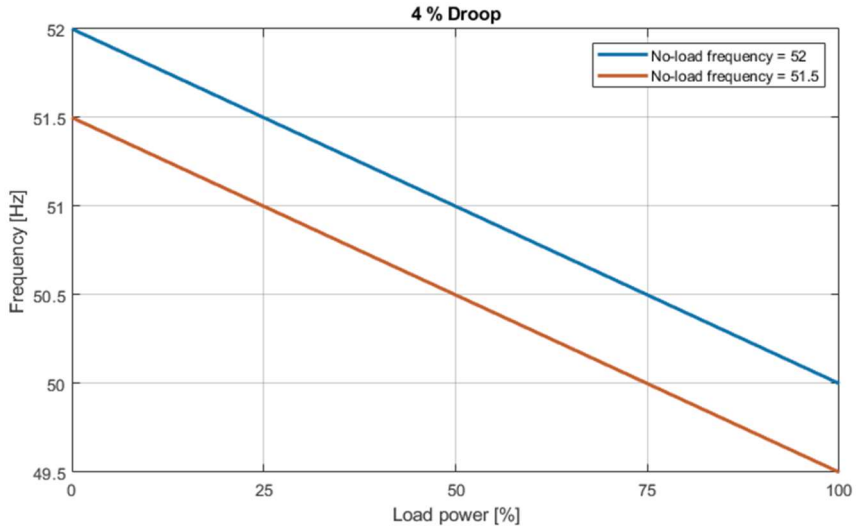

Figure 3-3: Speed-droop characteristics in a 50 Hz grid with 4 % droop setting.

3.2.1 Frequency operating standards and reserves

Power imbalances in a utility-scale grid are common, but typically they do not lead to any significant issues as the magnitudes of the deviations are small. However, if a larger deviation is to occur, different actions depending on the magnitude of the frequency deviation are to be realized to prevent significant harm to the operation of the system. The characterization of different frequency deviation magnitudes and normal operating range is a power system dependent problem. For example, in Finland and in the Nordics, the frequency is maintained at 50 ± 0.1 Hz by the primary frequency control systems. The regulation is realized by utilizing the frequency reserve market, where regulation services are provided as such:

1. Frequency containment reserve for normal operation (FCR-N), aims to keep the frequency in the normal range (49.9 – 50.1 Hz) by controlling power output as a function of frequency. Max. dead band ± 0.01 Hz, full activation in 3 minutes after ± 0.1 Hz step change.

2. Frequency containment reserve for disturbances (FCR-D), activation starts at ± 0.1 Hz and full activation when frequency deviation is ± 0.5 Hz or more. In a ± 0.5 Hz step change, 50 % activation in 5 s and 100 % activation in 30 s is required.

In addition to these, there are automatic (aFRR) and manual (mFRR) frequency recovery reserves, which are used for recovering the frequency back to the normal operating range and freeing the activated FCRs. [53] [54]

Due to the implications of decreasing inertia discussed before, a need for even faster frequency reserve has been recognized. The power system is dimensioned in a way that a loss of a single generation unit or a HVDC (High voltage direct current) link may not deviate the frequency under 49.0 Hz. According to Fingrid, the Finland national TSO (Transmission system operator), the fast frequency reserve (FFR) market was opened in May 2020. This means that generating facilities can participate in fast frequency regulation by offering the capacity of the power plant to the market. The reserve units are required to meet certain technical specifications and the compliance must be verified by prequalification tests. The required activation times for the units are listed in Table 3-1, where the reserve power provider can select any of the options that they want to provide. FFR requires the reserve to be active for at least 5 s, and the deactivation power ramp rate needs to be limited to 20 %/s, or if the activation time is 30 s or more, the ramp rate is not limited. The frequency measurement requirement for FFR states that the accuracy

must be within 10 mHz and the sampling time 0.1 s or less. Additionally, to better understand the state of the power grid in terms of inertia, a real-time inertia monitoring/estimation has been implemented throughout the Nordic TSOs' grids. This way, the worst-case power frequency disturbance can be evaluated beforehand. [2] [55] [56]

In a utility-scale grid, the grid ROCOF values even in larger disturbances are small enough that frequency measurements can be implemented with relatively slow sampling times and moving averages. For example, ENSTO-E suggests ROCOF withstand capabilities for different grid-connected applications as follows [57]:

- HVDC systems: ± 2.5 Hz/s (average for the previous 1 s),
- DC-connected power park modules: ± 2.0 Hz/s (average for the previous 1 s),
- Demand response units: No specified ROCOF value, but 500 ms measurement window allowed.

This means that, for example with 2.5 Hz/s ROCOF, the frequency has deviated only 0.05 Hz in 20 ms, which is well within the normal variation range of ± 0.1 Hz. This justifies the "slow" frequency measurement techniques discussed in Section 2.3. Additionally, as frequency, and especially ROCOF measurements typically include filtering, the initial maximum ROCOF introduced in Equation (3-5) may not be detected by these units. As stated in [57], ROCOF withstand capabilities are defined by analyzing a normative incident for the power system that led to a significant power imbalance / inertia loss. In smaller power systems, this normative incident could be defined by e.g., the loss of the largest generating unit.

Table 3-1: Activation options for fast frequency reserve units. [55]

Activation frequency (Hz)	**Maximum activation time (s)**
≤ 49.7	≤ 1.3
≤ 49.6	≤ 1.0
≤ 49.5	≤ 0.7

These operating standards and guidelines are well-defined for nation-wide electrical grids but when the power system is reduced to an islanded/isolated microgrid, the definitions and performances change radically. A microgrid needs to be able to operate in an islanded situation, where the main power grid has been disconnected. In islanded operation, the microgrid has a grid-forming unit, usually a generating set, that the rest of the system supports. However, diesel or gas –based gensets and the rest of the possibly renewable-based grid have a radically reduced inertia and are usually not effective enough in terms of frequency regulation in the presence of large power imbalances. Standalone gensets will undergo a relatively large speed/frequency deviation under these transients and this could introduce problems in the microgrid if no additional support is provided. Meeting conventional grid standard specifications for frequency (and voltage) fluctuations can be rather difficult (or impossible) in microgrids fed by these gensets [3]. Thus, these grid codes may not be applicable for islanded/isolated systems, but instead the operating limits need to be defined individually depending on the characteristics of the microgrid. For example, ISO 8528-5 standard specifies operating limit values for gensets of different performance class that include [58] [59]:

- steady-state frequency band,
- transient frequency deviation from nominal,
- frequency and voltage recovery time and
- many more regarding voltage etc.

These limits are much more relaxed when compared to operating limits for utility grids, for example, a G3 performance class genset's steady-state frequency band is defined as $< \pm 0.5$ %. As for load step performance of the generator, defined as load acceptance (increase) and load rejection (decrease), transient frequency deviation and recovery times are specified individually for both cases. Load rejection is based on 100% step load removal, but load acceptance is based on multiple load steps defined by the engine's break mean effective power (BMEP). BMEP is a theoretical performance parameter that describes the average pressure inside the cylinder. The ISO 8528-5 standard specifies six different load steps for each BMEP-rating from which the transient performance of the generator can be evaluated. For example, a G2 performance class genset transient frequency deviation in load rejection is $\leq +12$ % (of initial frequency) and in load acceptance the limit is ≤ -10 % (isochronous mode) and ≤ -15 % (droop mode). [58] [59]

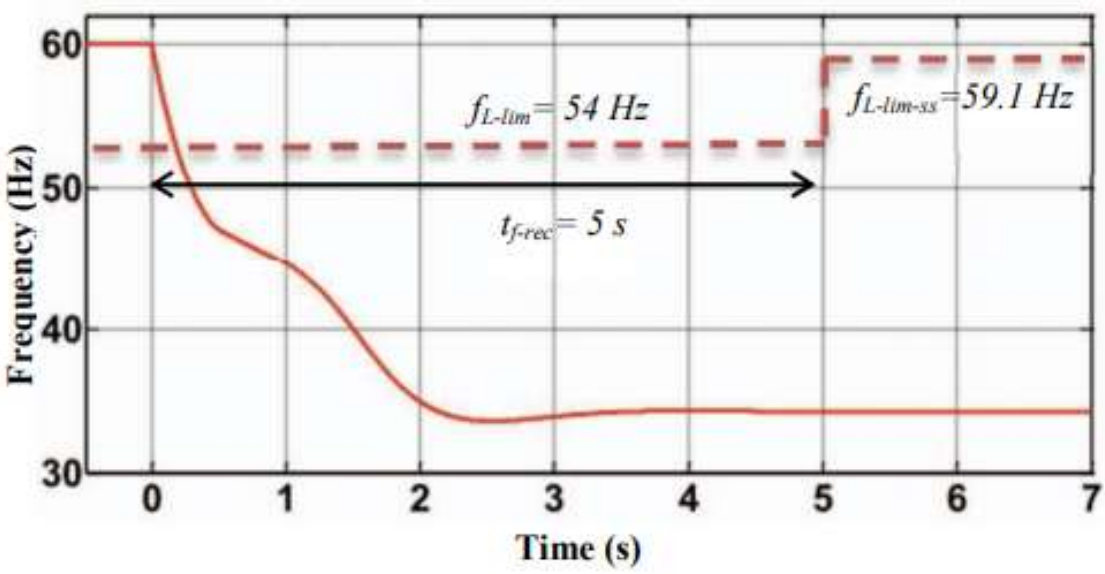

Figure 3-4: Frequency deviation of a microgrid fed by gensets subjected to a 70 % stepwise load increase. [60]

These genset specific limits can be used as a reference point for the islanded/isolated microgrid. Additionally, the gensets are frequently required to operate within customer expectations that might be even more demanding.

In [60], the problem during transient load changes with these types of gensets is demonstrated by a microgrid that has two natural gas gensets feeding the grid. The system is subjected to a 70 % load increase and the frequency deviation is shown in Figure 3-4. The figure also shows the frequency limits, $f_{L-\lim}$ (transient frequency deviation, BMEP load increase) and $f_{L-lim-ss}$ (steady-state frequency low limit) specified in ISO 8528-5 for G2 performance class. The time t_{f-rec} is the allowed recovery time for the frequency. It is clear from the figure that the requirements are not fulfilled as the system frequency collapses. This type of failure could be prevented by oversizing the gensets (more inertia) or for example using a underfrequency load shedding scheme. However, a 70 % load increase is a rather extreme event and typically this kind of performance is not expected from a system like this. A common approach for genset applications is to load the generator in multiple stages using automatic transfer switches or feeder switchgear. This allows the generator to gradually take smaller load steps and meet the required performance class specifications. Even though all the additional equipment will increase the cost of the system, it is still generally more cost-effective than oversizing the genset. [58] In the next section, an alternative way of improving the dynamics of the grid via energy storage systems is presented.

3.2.2 Frequency regulation with BESS and virtual inertia

High ROCOF situations may not be a concern in nationwide power grids with mainly large synchronous generators feeding the grid, but in much smaller islanded microgrid environments, the system's response to a power imbalance is much faster. To combat the stability problems in power systems introduced by low inertia, frequency regulation utilizing battery energy storage systems (BESS) (or supercapacitors) have been the subject of extensive research in the recent years [3] [9] [61 – 65] (to name a few). The fundamental idea behind frequency regulation with BESS is to provide the same kind of inertial response (as discussed in Section 3.1) that a conventional synchronous generator would have and thus essentially add *virtual inertia*. These systems are often called *virtual synchronous generators* (VSG) or *virtual machines* (VM). In addition to emulating inertia, the systems may be used for providing primary control of frequency. This is done by controlling the system in such a way, that the actions of a generator's prime mover governor are imitated. The active power output of the system is controlled based on the system frequency deviations and ROCOF, and thus supporting the grid stability in terms of frequency. Inertia emulation can also be used to support a microgrid in islanding transitions and usually the same BESS is used to provide voltage support via reactive power control. It should be noted that the source of the electrical energy does not particularly need to be a battery, it can be anything interfaced with a converter e.g., solar, wind turbines etc. [3] [9] [66] For example, some TSOs like Hydro-Quebec and EirGrid require all grid-connected wind farms to be capable of providing inertia services [67].

There is a multitude of different approaches regarding the implementation of virtual inertia, but the basic principle and function is the same. A sophisticated approach is to introduce a high-order model of an SG through mathematical modelling techniques, and to represent the dynamics of the generator as closely as possible. [3] For example, the Virtual Synchronous Machine (VISMA) method uses an SG modelled in synchronous reference frame and solves the underlying machine equations to imitate the dynamics [68]. A simpler way to implement virtual inertia is to utilize the swing equation (Equation 3-1) introduced in Section 3.1 to produce an approximation of the SG dynamics. The swing equation is solved for a phase command by the controller and the generated phase signal is then used in the PWM of the converter. [3] [69]

A frequency-power response -based control scheme can be used to achieve dynamic frequency control. The power command for the system is based on frequency deviation and the derivative of frequency i.e., ROCOF, which makes the system provide similar

response to that of an SG during inertial power release/absorption. The virtual inertia system's output power can be given as

$$P_{out} = K_D \Delta\omega + K_I \frac{d\Delta\omega}{dt} \quad (3\text{-}8)$$

where K_D and K_I are gains that represent damping and inertia, respectively, and $\Delta\omega$ is the angular frequency deviation of the system. Equation (3-8) consists of a droop part that focuses on achieving the steady-state value of frequency and reducing the frequency nadir after a transient power imbalance. The inertia-part or the derivative-part aims to react to the ROCOF and add a fast dynamic response to the imbalance, which is especially important in low-inertia microgrids since the ROCOF may rise to relatively high values right after the transient change in power. The power command from Equation (3-8) can be used to calculate the necessary current references for the converter control and thus a controlled power exchange between the virtual inertia system and the grid can be achieved. This scheme is relatively simple but requires accurate and fast tracking of the system frequency, and thus a careful design of the PLL is important. [3] In low-inertia islanded microgrids, the PLL performance may be inadequate, especially if the power quality is poor (harmonics, unbalances, etc.) as the frequency tracking requires filtering which then deteriorate the dynamics. Moreover, the derivative of the frequency is a term that is especially sensitive to noise and requires careful filtering and dead bands so that the system does not become unstable. As will be seen on the simulation and implementation part of this thesis, configuring all the necessary control parameters of this method is relatively difficult, at least in the case study.

Frequency droop-based control scheme is primarily developed for isolated microgrid operation and does not include ROCOF as a control input. The frequency droop can be presented as

$$\omega_g = \omega^* - m_p(P_{out} - P_{in}) \quad (3\text{-}9)$$

where ω_g and ω^* are the system and reference frequencies, respectively, P_{out} is the measured output active power, P_{in} is the active power reference and m_p is the power droop gain. This scheme typically includes a low pass filter for the output active power measurement, and as shown in [70], the system can then be approximated as a virtual inertia system, as in Equation (3-8). In addition to controlling the active power flow and subsequently the frequency, the microgrid droop methods typically include similar characteristics for voltage-droop. [3]

In [71], an improved droop-based topology was developed in which the droop gain in Equation (3-9) is changed as a function of ROCOF. In normal conditions, the controller acts as a traditional droop controller, but when ROCOF exceeds a certain threshold, the droop gain is modified. The system showed promising results as the frequency nadir in power imbalance situations reduced, as shown in Figure 3-5. However, as seen from the figure, the frequency has much more ripple when compared to the traditional droop response, which could indicate that the control gain for ROCOF was too high and this could lead to unstable responses. Utilizing non-linear droop curves and adaptive schemes can be more effective in low-inertia situations than traditional droop methods. For example, in [72] an adaptable droop scheme showed increased stability versus a linear droop method. The droop gain in this study is proportional to the frequency deviation which made the output power response non-linear. Additionally, the scheme included a fast secondary integral controller to move the power set point according to the changed system conditions. A non-linear droop method is also considered in the simulation part of this work in Chapter 4, which also shows some improvements when compared to the traditional linear droop.

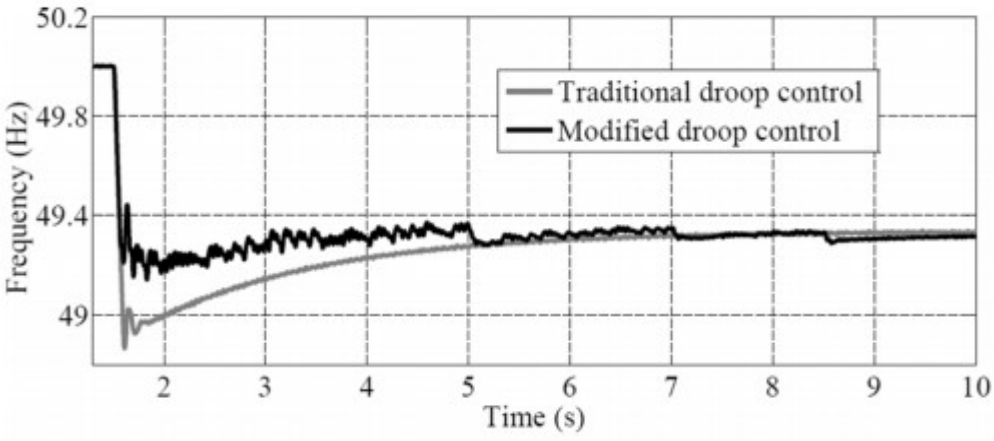

Figure 3-5: System frequency response to a sudden microgrid islanding using traditional droop control and a modified droop control. [71]

3.3 Eaton EnergyAware UPS and UPS-as-a-Reserve

The importance and demand of data centers is increasing rapidly as data-oriented technologies advance. Consequently, as data centers require a lot of energy, currently approximately 1 % (205 TWh) of all consumed electricity world-wide [73], there is a clear trend for energy demand increase. These data centers are very dependent on continuous supply of power, as even sub 100 ms interruption may be critical, and therefore they are always equipped with UPS systems to ensure reliable operation. As these UPS systems are designed to have redundancy and flexibility (see Figure 2-2), there is a lot of potential for demand response participation and frequency regulation [74] [75]. UPS manufacturer Eaton has developed their data center -oriented EnergyAware UPS systems with the so-called UPS-as-a-Reserve (UPSaaR) technology to enable the devices to participate in primary frequency response. This way, the UPS investment for the data center can generate some revenue by offering balancing services to the market. [12]

The basic idea of UPSaaR is to control the UPS power demand based on the present power balance situation and frequency. When the system frequency decreases below a certain threshold, the UPS can either shift the data center load to the battery by cutting off the grid (islanding) or even supply power back to the grid through the bi-directional converter (dynamic upwards regulation). The power shifting does not need to be complete, meaning that the critical load can also be supported partially by the batteries and thus reducing the load as a function of frequency. The power flow of the system during full dynamic upwards regulation is presented in Figure 3-6, where the UPS has 50 % critical load, and the rest of the available power is fed back to the grid. If the power system frequency rises, the system can also enable down-regulation. In this case the UPS increases its power demand by charging the batteries. The charging current can also be controlled as a function of frequency. For the down-regulation to be possible, the UPS batteries need to be only partially charged, in which case Li-ion batteries are preferred. [10] [12]

The regulation power may be requested by the TSO or an aggregator, or they may be calculated based on the frequency measurements on site. In order to ensure reliability, the state-of-charge (SoC) of the battery is first evaluated before any regulation actions. Additional on-site back-up generators can be started, if the disturbance lasts longer and the battery SoC gets too low.

The performance of the dynamic regulation ability of the UPS was demonstrated in Swedish TSO’s prequalification tests for FCR-D. The frequency deviation was simulated by

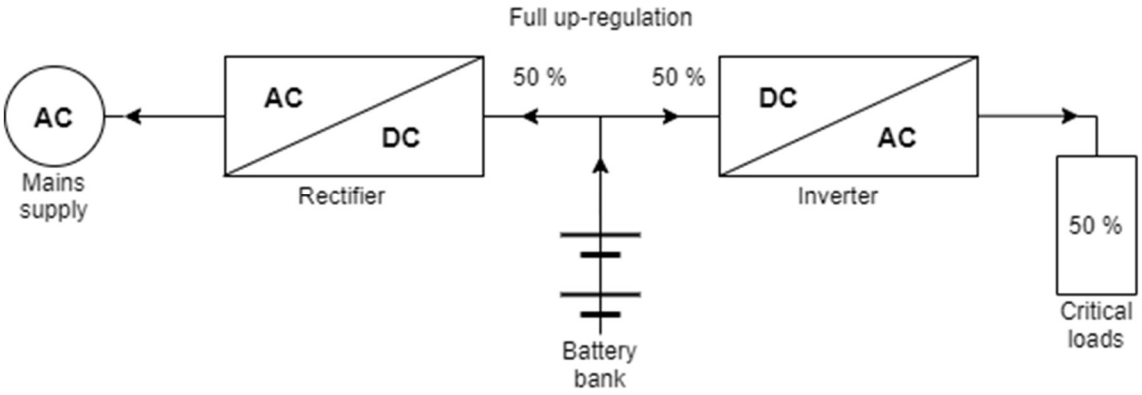

Figure 3-6: Power flow during full upwards dynamic regulation.

generating a test signal that decreased in frequency from 49.9 Hz to 49.5 Hz in 0.05 Hz steps and increased back to 49.9 Hz in a similar fashion. The test showed that the UPS fulfilled the FCR-D activation requirements. In addition to that, the reaction speed has been benchmarked in a laboratory environment, where a 200 kW UPS fed 100 kW of load and an activation signal via CAN burst was given to the system to activate the regulation function. An oscilloscope capture of the test is shown in Figure 3-7, where it can be seen that quickly (within one 50 Hz cycle) after the CAN burst, the UPS started to draw energy from the batteries (indicated by the battery current). In addition to supplying the 100 kW critical load, the UPS fed the redundant 100 kW back to the grid, as seen from the phase angle shift of the input current. [10]

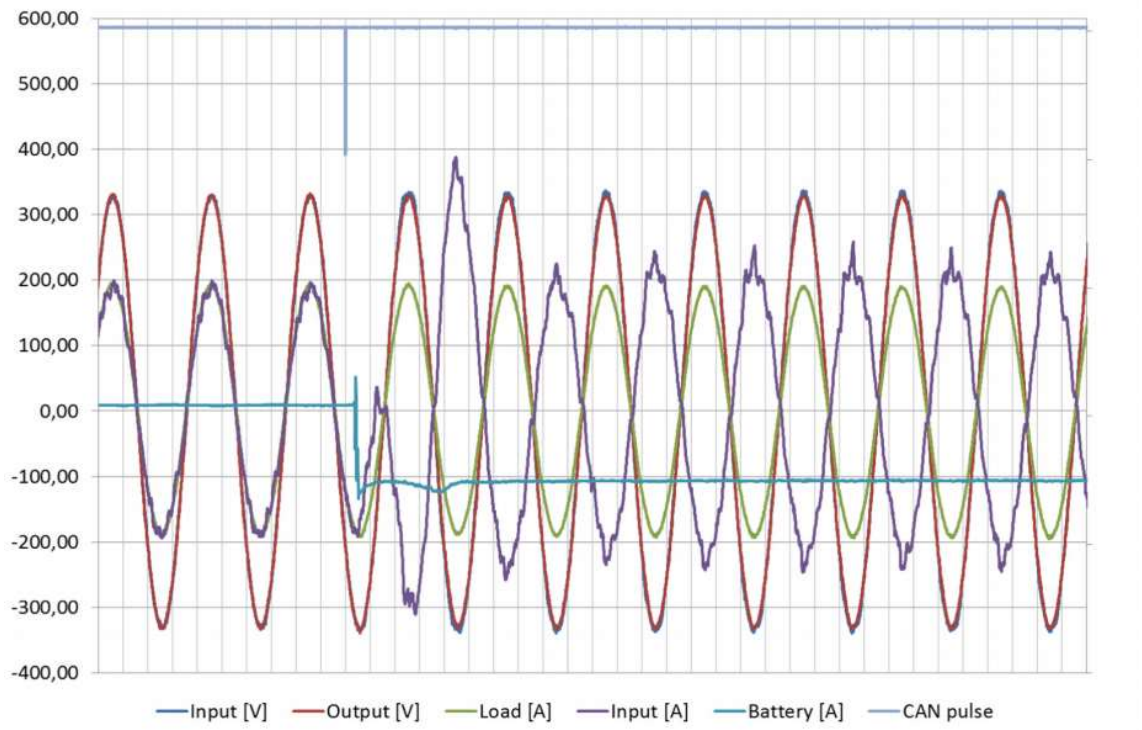

Figure 3-7: Results from the reaction speed benchmarking test of the UPSaaR functionality in a 200 kW UPS. [10]

4. DEVELOPING AND SIMULATING FREQUENCY REGULATION METHODS IN A LOW-INERTIA MICROGRID

The capability and performance of UPS devices in frequency regulation has been demonstrated within the context of conventional, utility-scale power systems. However, as discussed in the previous chapter, reducing the power system inertia makes the regulation task more challenging as the frequency transients get faster. Whether the reduced inertia is due to large SGs replaced by renewables or due to the reduced size of the power system (microgrid), the control problem is the same: the regulation needs to be faster.

As a continuum to the Eaton *EnergyAware* technology (UPSaaR), a faster regulation algorithm is developed with extremely low-inertia power systems in mind. In this case, the low-inertia system is a diesel genset feeding some arbitrary resistive loads and the UPS. The case study power system could be a data center microgrid that either has been islanded as a consequence of a utility fault, or an intentionally isolated system. Regardless, the idea is to support the UPS input-side generation capacity, i.e., the generators to survive frequency deviations caused by load steps. The UPS input-side could for example have some other auxiliary data center related loads that are not protected by the UPS or the microgrid could also be a larger system with only some of the load being protected by UPS systems, as presented in Chapter 1, Figure 1-1.

In this chapter, a simulation model of the isolated microgrid is constructed of which the main components are the diesel generating set, the UPS rectifier circuit and its controls and the loads. First, the model of the genset is described and some of the simplifications are justified and explained. Secondly, the UPS rectifier model is briefly introduced, and the entirety of the simulated power system is presented. After the simulation environment is established, a frequency measurement method is implemented into the PLL function in the rectifier. Lastly, a couple of frequency regulation methods are tested and benchmarked by simulating resistive load steps in the feeding grid. These results can then be used as a reference to the laboratory environment measurement tests later in Chapter 5.

4.1 Diesel generating set model

The primary electrical energy source in the simulated system is a standby diesel generating set, which is used to feed the load and the UPS device. The genset and the rest of the system is an isolated power system, meaning that there is no connection to an external electrical grid. This way, a low-inertia or weak grid can be emulated, and the back-up operation and performance of the generator can be evaluated. It should be noted that the focus of this thesis is not on simulating the generator system accurately, it is merely a platform to benchmark the frequency regulation algorithm for the UPS device.

The generator modelling is first based on pre-existing measurement data from load step testing of a 1000 kVA diesel genset. The measurement data is the generator output three-phase voltages captured by an oscilloscope from different sized load steps. The voltage measurements are used to calculate the frequency of the output voltage during the load step, which is then used as a reference in constructing a generator model with similar type of response.

The generating set system model is shown in Figure 4-1. It consists of a synchronous generator block, 'Synchronous Machine pu Standard', from MATLAB Simulink powerlib block library, IEEE AC1A[2] excitation system block and a subsystem for the engine dynamics and speed governor. The SG is modelled in *dq*-reference frame and is set to have its mechanical input as mechanical power P_m. The electrical parameters of the synchronous generator are set according to the data sheet of the 1000 kVA generator, see Appendix A.

The IEEE AC1A excitation and voltage regulator system was chosen as it seemed to be accurate enough and no separate power system stabilizer circuit is implemented to the excitation model as it does not provide any additional benefit to the simulation. A simple under frequency roll-off (UFRO) feature is implemented to the voltage regulator by setting the voltage reference to be directly proportional to the rotational speed (or the frequency) of the generator. The UFRO feature essentially provides additional protection against under-speed of the generator by reducing the output voltage amplitude when the generator speed has slowed down below a certain threshold called a *knee-point*. The Volts/Hz characteristics of the generator voltage regulator is shown in Figure 4-2.

[2] IEEE AC1A is an excitation system from the IEEE 421.5 standard, which is used to produce the field voltage for the generator [76].

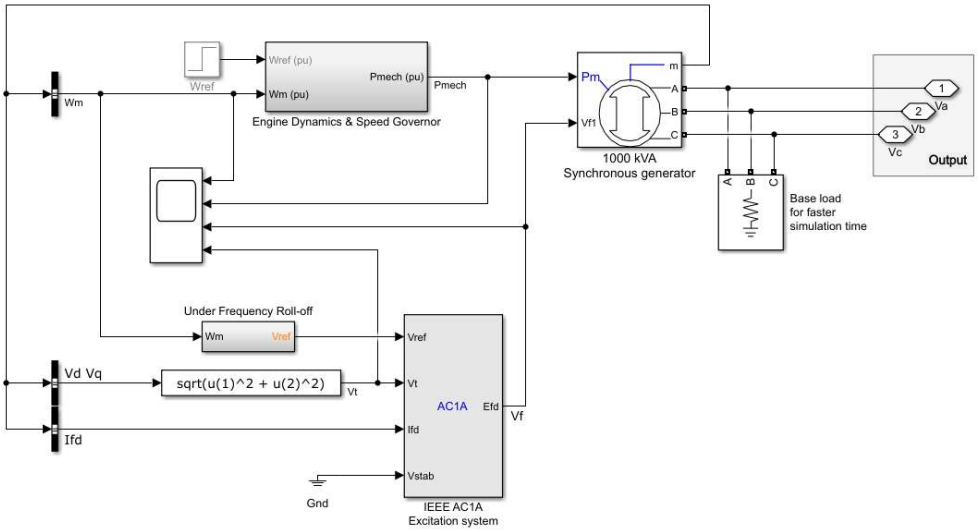

Figure 4-1: Diesel generating set model.

The most important part of the genset simulation in the context of this thesis was the engine dynamics and speed governor as they relate to the frequency regulation of the system. The inputs of this subsystem are the reference rotational speed and actual measured rotor speed. The speed governor is controlled in isochronous mode by a PI-controlled feedback loop such that the rotational speed is maintained at 1500 RPM. The engine dynamics are simply represented with a delay block and dynamic rising rate limit, which were parametrized by trial and error. After passing through the regulator and the engine dynamics, the resulting torque can be used to calculate the mechanical power of the engine as the output of the subsystem.

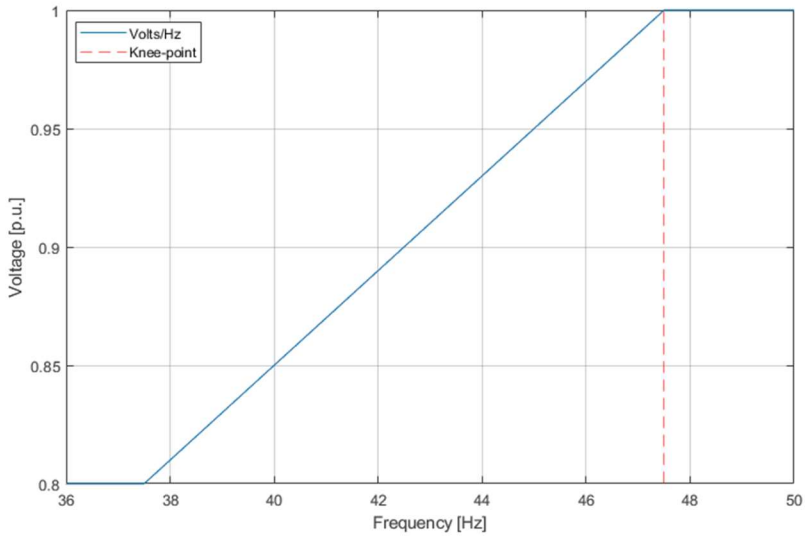

Figure 4-2: Volts/Hz characteristics of the generator voltage regulator.

The 1000 kVA generator model is first used as a placeholder and reference so that the operation of the UPS and the frequency regulation system can be initially verified. After that, as measurement data is captured from the laboratory testing of the smaller 250 kVA generator, the model is updated accordingly. The 250 kVA generator is modelled the same way as the 1000 kVA generator, only some of the parameters are adjusted to match the performance. The relevant genset parameters are presented in Appendix A.

4.2 UPS rectifier and power system model

The power system Simulink model is presented in Figure 4-3. The UPS system model consists of a three-level converter as discussed in Chapter 2, its control system, input capacitors and chokes (inductors) and the DC-link with DC capacitors and the load. Additionally, the BESS is connected to the DC-link, and is simply represented by an ideal controllable current source. The inverter and output side of the UPS is not included in the simulation, rather the resistive loads LOAD+ and LOAD- connected to the DC-link represent the UPS output load. The feeding grid of the UPS system simply consists of some line impedance and the resistive load step bank which is implemented by controlling a three-phase circuit breaker to connect and disconnect the load.

The top-level control system of the UPS is presented in Figure 4-4. Three measurements are taken from the power system circuit: rectifier input voltage (*Vrec*), input choke current (*Irec*) and DC link voltage (*Vlink*). These measurements are passed through analog and digital filters, and eventually used to control the UPS rectifier. The PLL uses the three-phase voltage as an input and extracts phase angle data for the rectifier control system. The PLL is also used to calculate the frequency and the ROCOF of the input voltage for the actual frequency regulation algorithm. The PWM gate signals are also passed

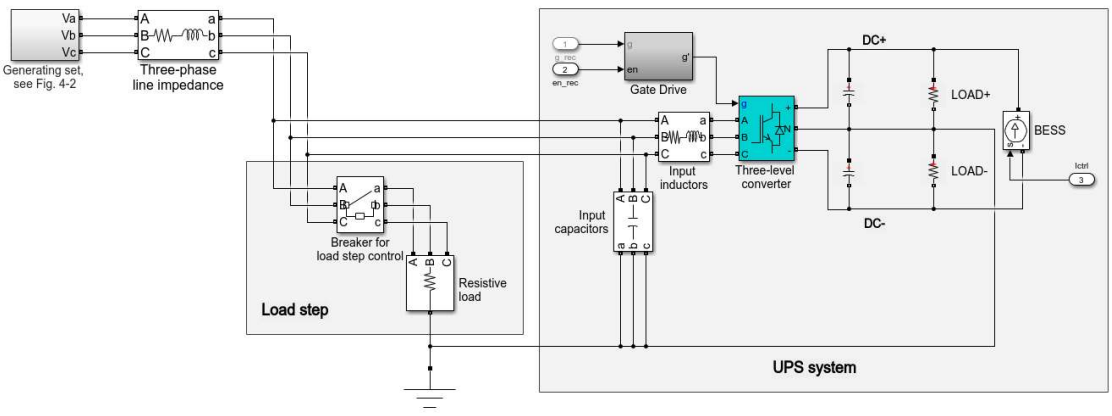

Figure 4-3: Power system circuit model in Matlab Simulink

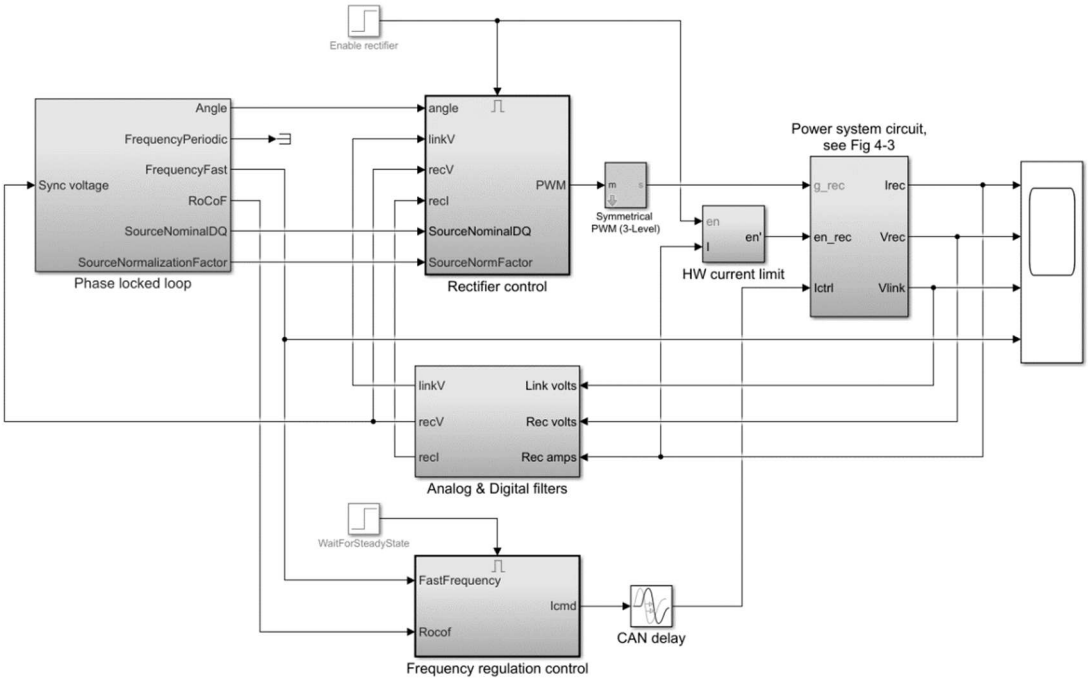

Figure 4-4: The control system of the UPS rectifier

through a gate drive block in Figure 4-3 and the rectifier current can then be limited by the hardware current limit block.

The UPS model is controlled as a singular unit even though in reality this type of UPS consists of multiple power modules that each has its own rectifier circuits and control systems. For simplicity's sake, the power modules in this simulation are assumed to operate identically and no internal load sharing problems are considered. As for the frequency regulation algorithm, the power/current command includes a small delay that represents the inherent CAN-bus delay that could be present in the real-world application. No additional dynamics are considered in the BESS or the control system.

4.3 Frequency measurement and filtering considerations

The frequency measurement that is used as a control input to the frequency regulation algorithm is calculated in the dq-PLL function. The PLL function is run in a 2250 Hz loop meaning that the frequency is sampled every $\frac{1}{2250} = 444\ \mu s$. The frequency calculation f_{fast} is based on the angle correction adjustments to the base frequency as follows:

$$f_{fast} = \frac{\theta_{corr}\, f_{sw}}{2\pi} + f_{base}\,, \qquad (4\text{-}1)$$

where θ_{corr} is the angle correction made by the PLL function, f_{sw} is the switching frequency of the converter, in this case $f_{sw} = 8 \cdot f_{PLL} = 8 \cdot 2250\ \mathrm{Hz} = 18\ \mathrm{kHz}$ and f_{base} is the base frequency of the PLL. This allows very fast tracking of the input frequency but may also introduce unwanted noisy ripple to the measurement, which could jeopardize the robustness of the control algorithm. The noise originates from any harmonics or unbalances in the tracked voltage. Figure 4-5b shows the estimated frequency directly calculated from the angle corrections in a stepwise change in two cases: with and without voltage harmonics. Table 4-1 shows the harmonic content in the "harmonic-polluted" example case, and the related three-phase voltage waveform is shown in Figure 4-5a.

Table 4-1: Harmonic content in the tracked voltage.

Harmonic order	Magnitude (%)
1 (fundamental)	100
2	2
3	5
4	1
5	6
6	0.5
7	5
8	0.5
9	1.5
10	0.5
11	3.5

The frequency measurement has a large amount of high frequency ripple that renders the measurement unusable in the case of voltage polluted by harmonics. The situation gets even worse if there are phase unbalances. Conversely, when the voltage is free of harmonics, the frequency tracking is accurate as the steady-state error is negligible. Also, the measurement settles within 0.1 Hz in less than 100 ms and the fall time (90 % to 10 % of the step) is approximately 10 ms.

Even though the focus in this case study was not on harmonic-polluted voltages, they are still considered to make the simulation more realistic. To attenuate the high frequency noise caused by the harmonics, the calculated frequency needs to be low pass filtered. A second-order Butterworth[3] low pass filter (LPF) is designed with MATLAB. The cut-off frequency of the filter is set to 40 Hz, which was determined to be suitable after some testing. As the whole control structure is digital, the filter is discretized with the Tustin's method (bilinear transform) and a sampling frequency of 2250 Hz. From the discretized transfer function model of the filter, a second-order section form is generated, and these scalars can be used to construct a digital biquadratic filter in Simulink. The biquadratic filter scheme is shown in Figure 4-6, and the filtered frequency with harmonic-polluted voltages is shown in Figure 4-5c.

The main concern in implementing a LPF is that the dynamics of the measurement will get slower and the advantages of the faster frequency measurement are diminished. However, even with the added LPF, the frequency settling time in the 5 Hz step is just over 100 ms and the fall time is approximately 13 ms. It should be noted that in the context of this case study, the frequency measurement is not at all aimed to be optimal and for example, even the filtered voltage in Figure 4-5c has a steady-state peak-to-peak ripple of ~0.1 Hz. In the case of large frequency deviations in isolated microgrids studied in this thesis, this does not cause issues, but the accuracy does not fulfill the requirements of for example the Fingrid FFR.

In addition to the frequency measurement, ROCOF is also used as a control input in the frequency regulation algorithm. ROCOF is calculated by an additional differentiation of the frequency and therefore is extremely sensitive to disturbances. Consequently, the ROCOF measurement is implemented with an additional second-order LPF, which is designed the same way as the frequency filter.

[3] A type of signal processing filter that aims to have a flat passband frequency response.

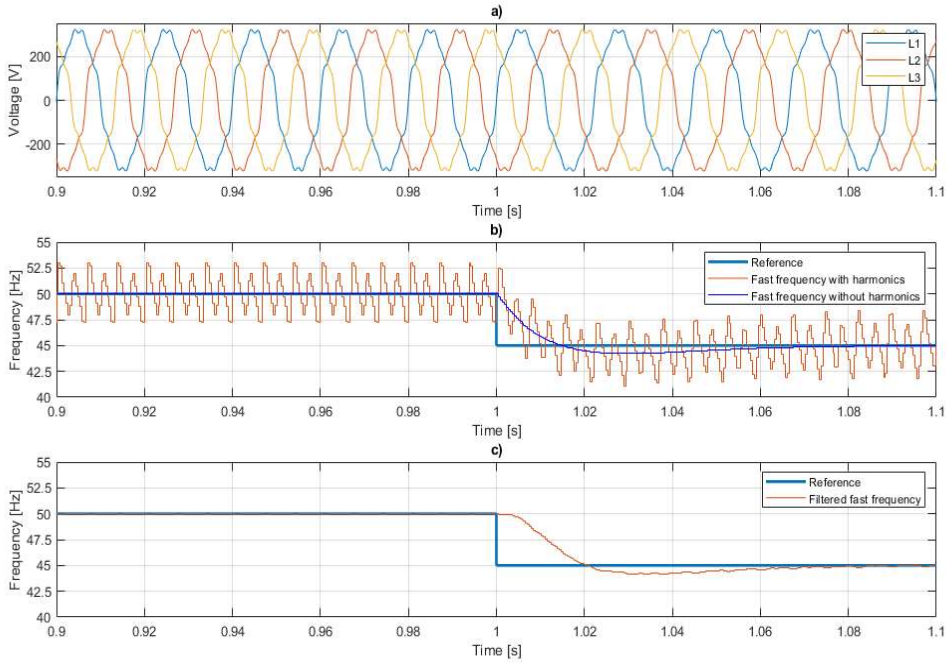

Figure 4-5: a) The tracked three-phase voltages with harmonics as presented in Table 4-1. b) PLL fast frequency measurement with and without harmonics in a 5 Hz step. c) PLL filtered fast frequency measurement with harmonics in a 5 Hz step.

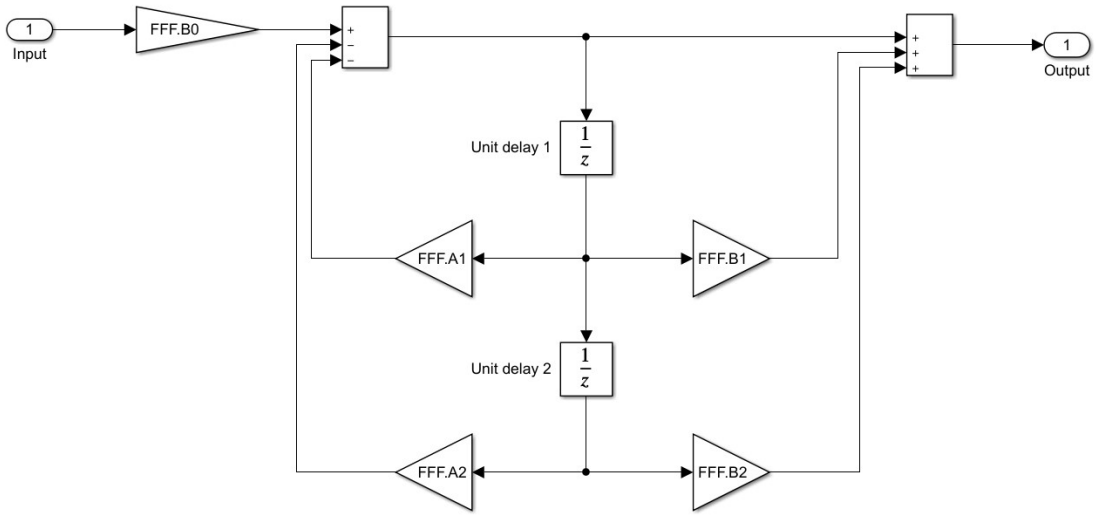

Figure 4-5: Second-order digital biquadratic filter scheme in MATLAB Simulink. The FFF.A and FFF.B gain coefficients represent the filter's poles and zeros.

4.4 UPS frequency regulation methods and performance

Now that the sub-cycle frequency measurement is established, the frequency regulation algorithm can be developed. As stated earlier, the goal is to calculate appropriate power responses to the frequency deviations detected by the PLL. The response in the simulation, and later in the actual implementation, essentially is a power command for the BESS in the UPS, i.e., the algorithm tells the system how much power is drawn from the BESS. The power from the BESS can be either fed back to the feeding power system, or it can be used to support the critical load of the UPS, which in effect reduces the load experienced by the feeding system. This allows the system to undergo much bigger load steps and reduces the rapid frequency deviations, which could cause issues in the power system. In the context of this thesis, only so-called up-regulation is considered which means the algorithm only considers negative frequency deviations i.e., frequency dips.

The performances of the frequency regulation algorithms are evaluated by applying different sized load steps into the input side of the UPS device. The power system frequency, ROCOF and three-phase voltages are measured and used as performance-metrics. As a reference performance of the genset, three sets of resistive load steps are simulated with the frequency regulation disabled. The frequency responses of the 100 kW, 160 kW and 100 to 200 kW load steps are shown in Figure 4-7, Figure 4-8 shows the respective ROCOF measurements and Figure 4-9 shows the voltage *d*-component (amplitude) during the event. Additionally, the amount of active power, or the energy, injected into the input side of the grid is analyzed since it represents the effectiveness of the regulation method. The regulation methods are also tested with different parametrizations to achieve the optimal response.

In the simulation part of the work, a couple of slightly different approaches were studied: linear droop, virtual inertia or ROCOF-control, and piecewise linear-elliptic droop. These methods have the same basic principle, but some differences can be seen in the performance as described next.

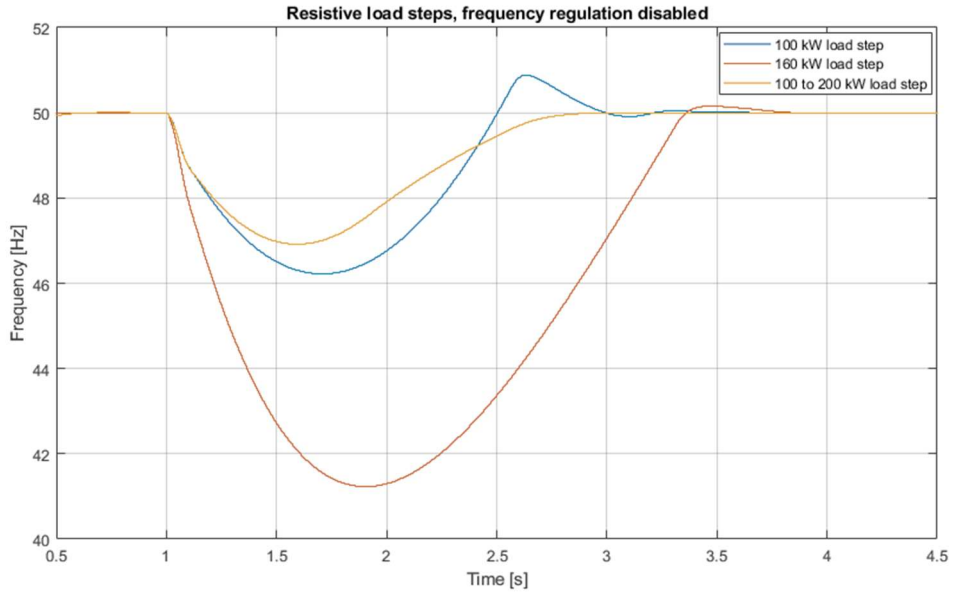

Figure 4-7: Power system frequency measurement after resistive load steps (100 kW, 160 kW and 100 to 200 kW) at time step 1 s.

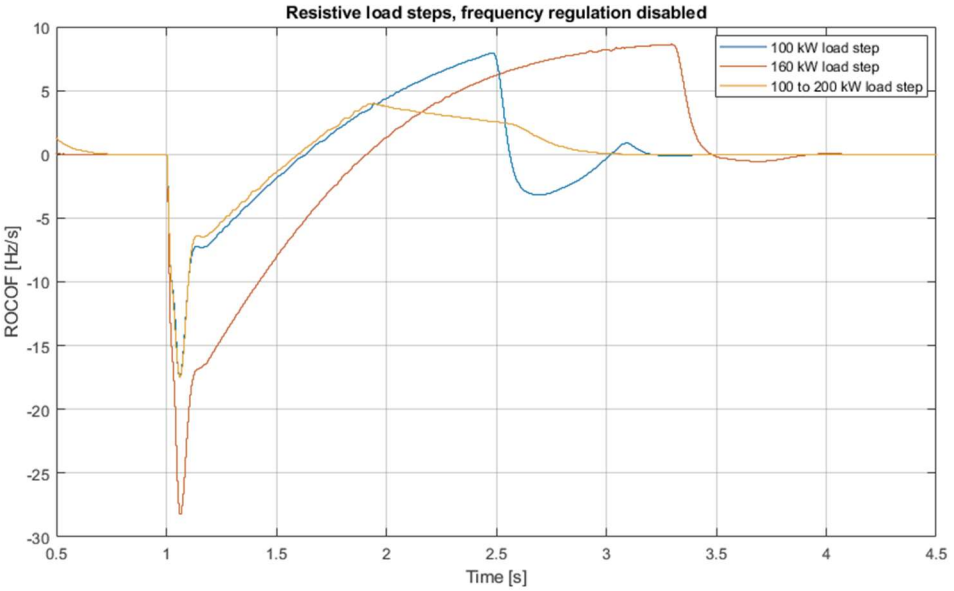

Figure 4-8: ROCOF measurement after resistive load steps (100 kW, 160 kW and 100 to 200 kW) at time step 1 s.

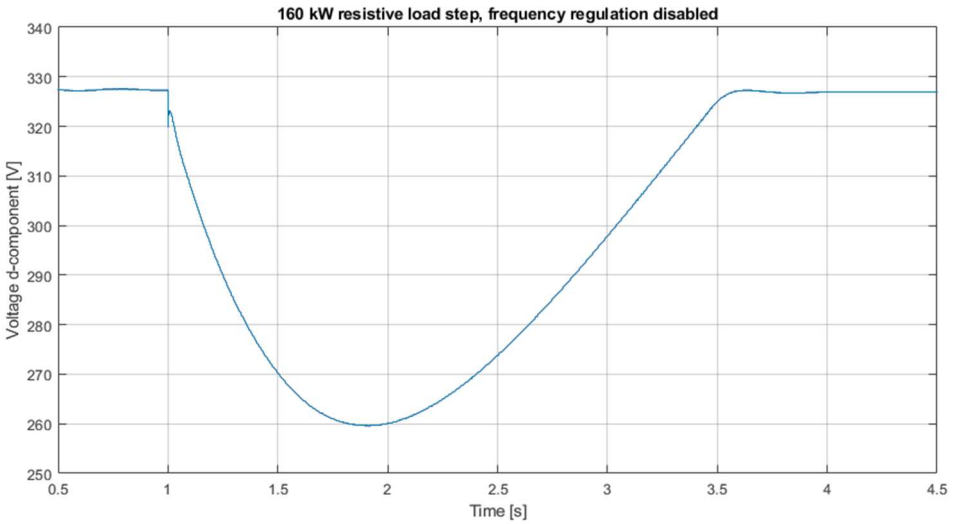

Figure 4-9: Grid voltage d-component after a 160 kW resistive load step at time step 1 s.

4.4.1 Linear droop

The simplest method to regulate power system frequency is to implement a linear frequency droop control. This method only uses frequency as a control input, which is used to calculate the necessary power commands, *PTarget*, as shown in the droop curve in Figure 4-10. The droop curve includes a couple of key parameters that are used to configure the frequency regulation algorithm. First of all, the nominal frequency can be configured and a frequency dead band around the nominal frequency can be set so that unnecessary power commands are not calculated when the frequency deviations are small. This dead band is set with the parameters *LowStart* and *HighStart* but in this case, the down-regulation side of the curve (right side of the Figure 4-10) can be forgotten as only up-regulation is considered. When the frequency deviates out of the dead band, the initial power command can be configured with *RampStart*. The actual droop curve is defined by the maximum power that can be drawn for regulation, *MaxDRPowerPercentage*, and the respective minimum frequency, *LowMax*. The MATLAB Simulink implementation is done with a simple look-up table as shown in Figure 4-11.

The performance of the linear droop method is demonstrated in Figures 4-12 – 4-14, where 100 kW, 160 kW and 100 to 200 kW load steps are applied, and the respective system frequencies are plotted. The figures also show the frequencies during the same load step when the regulation is disabled as in Figure 4-7, and the active power drawn from the UPS. As can be seen from the figures, the system frequency response is greatly improved as the frequency nadir is increased by 4.7 % (100 kW step), 17.8 % (160 kW s and 6.3 % (100 to 200 kW step). The time it takes for the frequency to set back to within

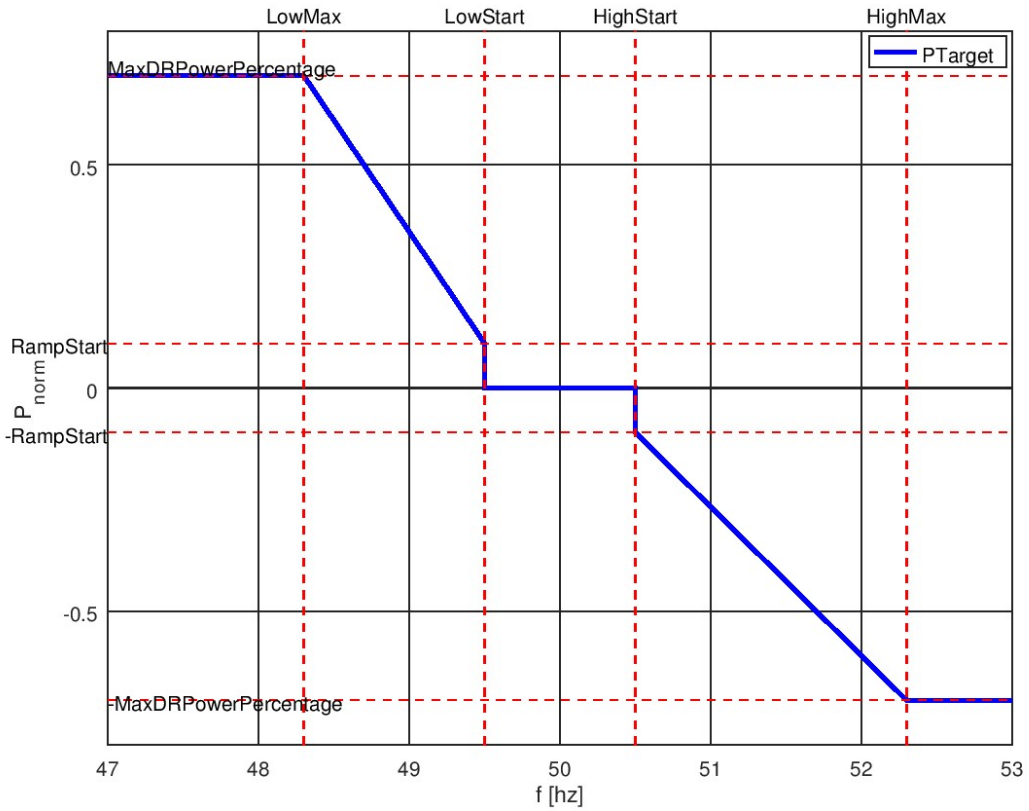

Figure 4-10: Droop curve for the frequency regulation algorithm.

0.1 Hz of nominal is also reduced. The active power drawn from the UPS has a quick peak of around 75 % of the load step, after which it gradually decreases back to zero. The entirety of the event only lasts for 1 – 2 seconds, which also means that not a lot of energy needs to be drawn for the regulation to operate successfully. Figure 4-15 shows the grid voltage *d*-component during the 160 kW step. Clear improvements can also be seen in the voltage, but this is mainly due to the genset UFRO not decreasing the output voltage so much, as the frequency dip is less extreme.

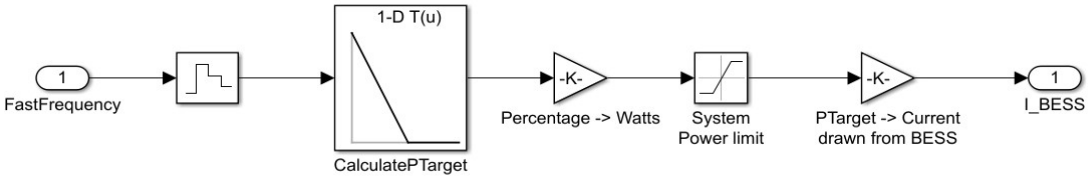

Figure 4-11: MATLAB Simulink implementation of the linear droop method.

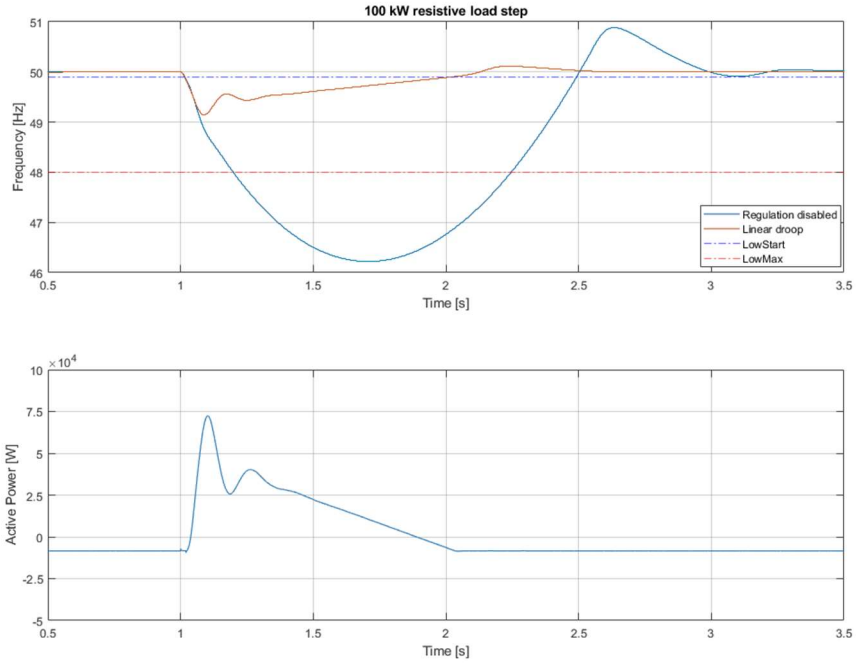

Figure 4-12: System frequency and active power from the UPS after a 100 kW resistive load step with linear droop enabled. LowStart = 49.9 Hz (blue dotted line), LowMax = 48.0 Hz (red dotted line), RampStart = 0 % and MaxDRPowerPercentage = 100% (200 kW).

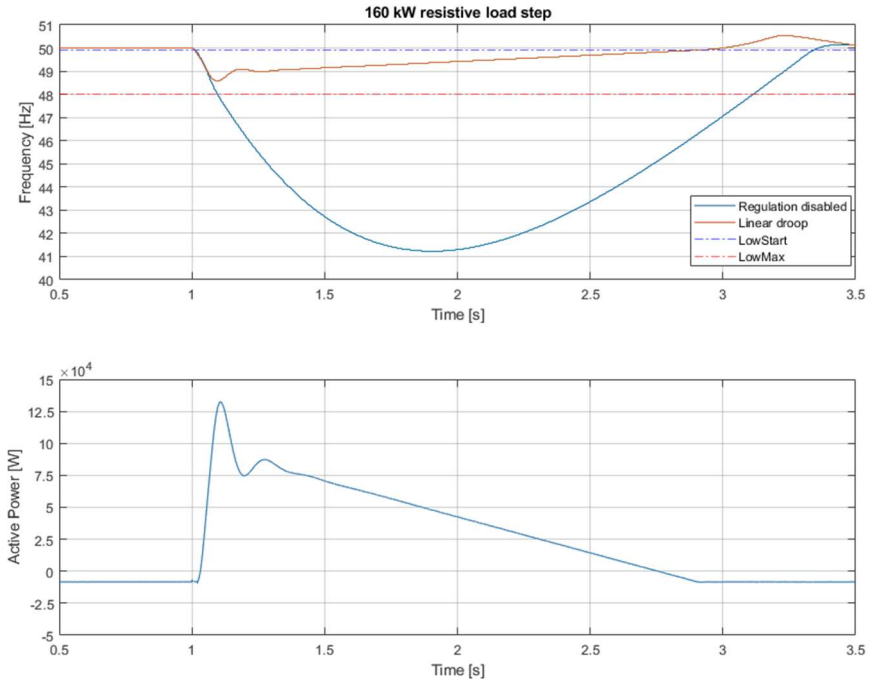

Figure 4-13: System frequency and active power from the UPS after a 160 kW resistive load step with linear droop enabled. LowStart = 49.9 Hz (blue dotted line), LowMax = 48.0 Hz (red dotted line), RampStart = 0 % and MaxDRPowerPercentage = 100% (200 kW).

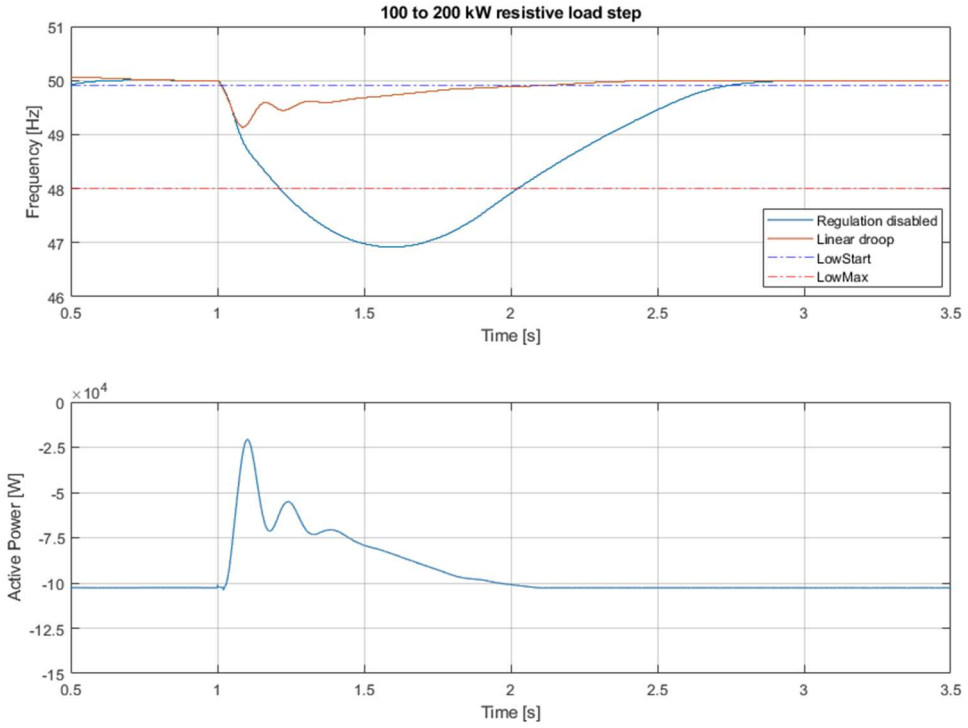

Figure 4-14: System frequency and active power from the UPS after a 100 kW to 200 kW resistive load step with linear droop enabled. LowStart = 49.9 Hz (blue dotted line), LowMax = 48.0 Hz (red dotted line), RampStart = 0 % and MaxDRPowerPercentage = 100% (200 kW).

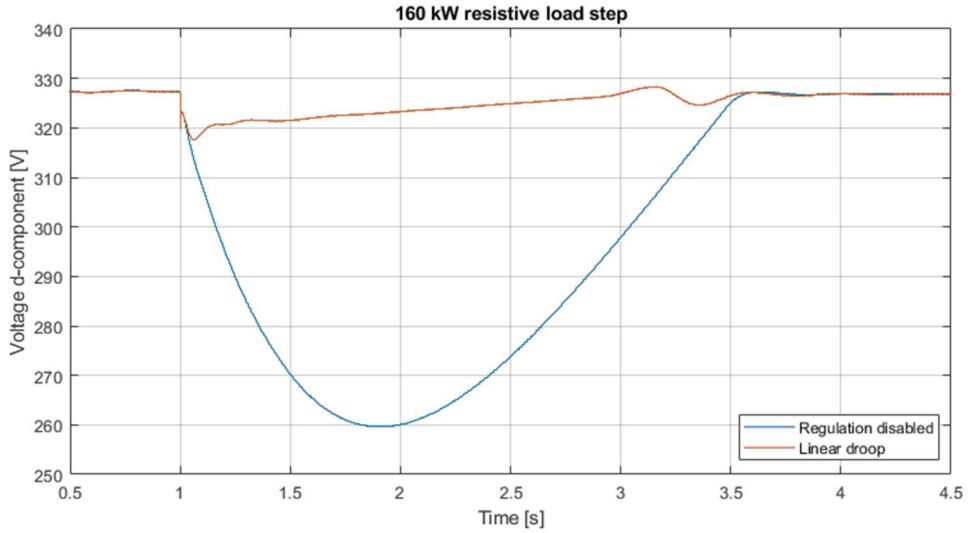

Figure 4-15: Grid voltage d-component after a 160 kW resistive load step.

The linear droop performance demonstrated in Figures 4-12 – 4-14 uses fairly reserved configuration regarding the *LowStart* and *LowMax* parameters, but also all of the availa-

ble UPS power is used in frequency regulation. Another way of approaching the configuration is to set *MaxDRPowerPercentage* to a lower value but allow the droop curve to be steeper, i.e., setting the *LowStart* and *LowMax* parameters higher. It should be noted that setting the *LowStart* parameter should be done carefully to prevent excessive regulation during normal frequency deviations. Therefore, *LowStart* is left to the default value of 49.9 Hz, but *LowMax* is now increased to 49.5 Hz. *MaxDRPowerPercentage* is lowered to 60 %, which means that only 120 kW is available for regulation purposes. The results from a 160 kW load step are shown in Figure 4-16, which also includes another parametrization with *LowMax* at 49.0 Hz and *MaxDRPowerPercentage* at 100 %. The results show that only <1 % improvement can be achieved with the different settings and in the case plotted with red color, the response starts to show oscillations, which indicates possible instabilities.

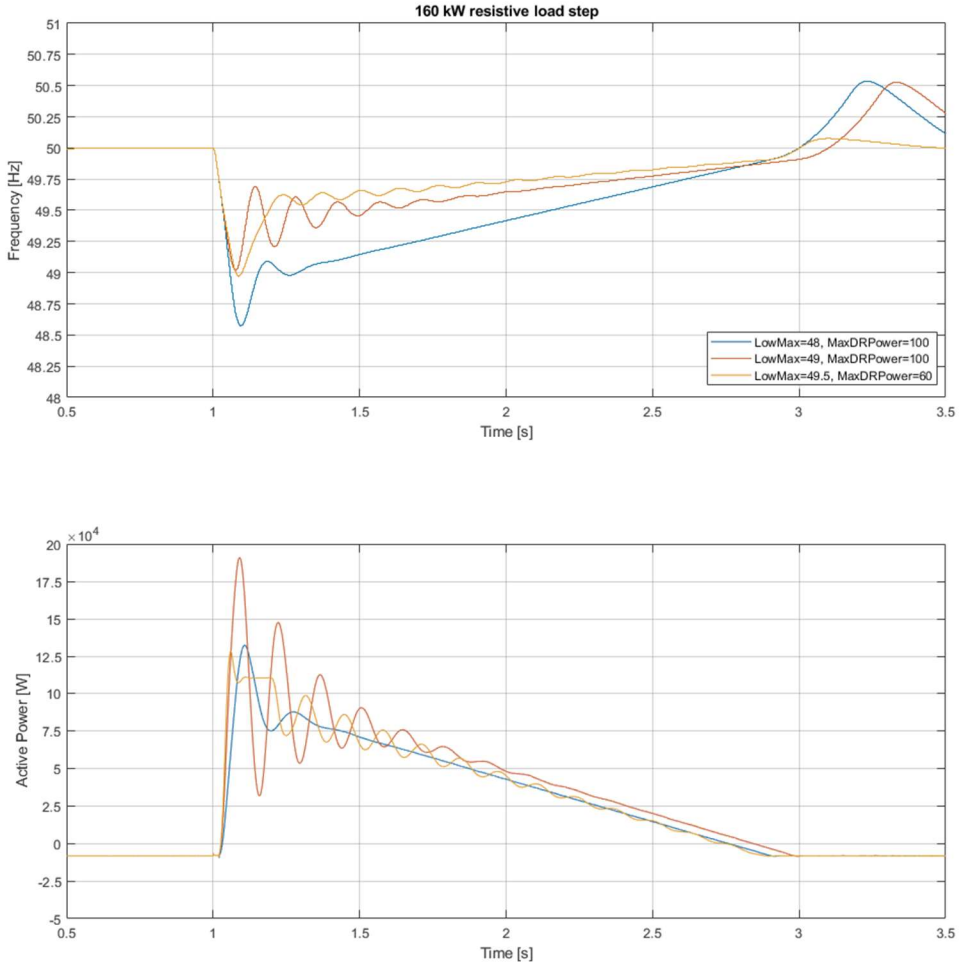

Figure 4-16: System frequency and active power from the UPS after a 160 kW resistive load step with linear droop enabled. Three different parametrizations for the linear droop: LowMax = 48, MaxDRPower = 100, LowMax = 49, MaxDRPower = 100 and LowMax = 49.5, MaxDRPower = 60. LowStart is set to 49.9 Hz in all the cases.

4.4.2 Virtual inertia or ROCOF-control

In low-inertia power systems, for example in the islanded diesel genset driven system this thesis studies, the frequency deviations due to load steps are fast and the frequency regulation algorithm needs to respond immediately after the load is connected. The linear droop method requires a dead band around the nominal frequency which means that when a load step is applied, there is a short time before the regulation reacts to the event. This delay is increased, if the system frequency before the event is above the nominal and the gap to the *LowStart* frequency is bigger. This issue is illustrated in Figure 4-17, where a delay of approximately 70 ms can be seen, before the *LowStart* frequency is reached.

In order to speed up the power response, ROCOF is added as a control input to the regulation algorithm and the power command is now calculated as in Equation (3-8). The frequency droop part of this method stays the same as described above, and the same type of droop curve is used for the ROCOF as well. The regulation can now be set in such a way, that even if the system frequency is above nominal before the load step, the regulation can react to the event before the frequency has decreased to *LowStart*.

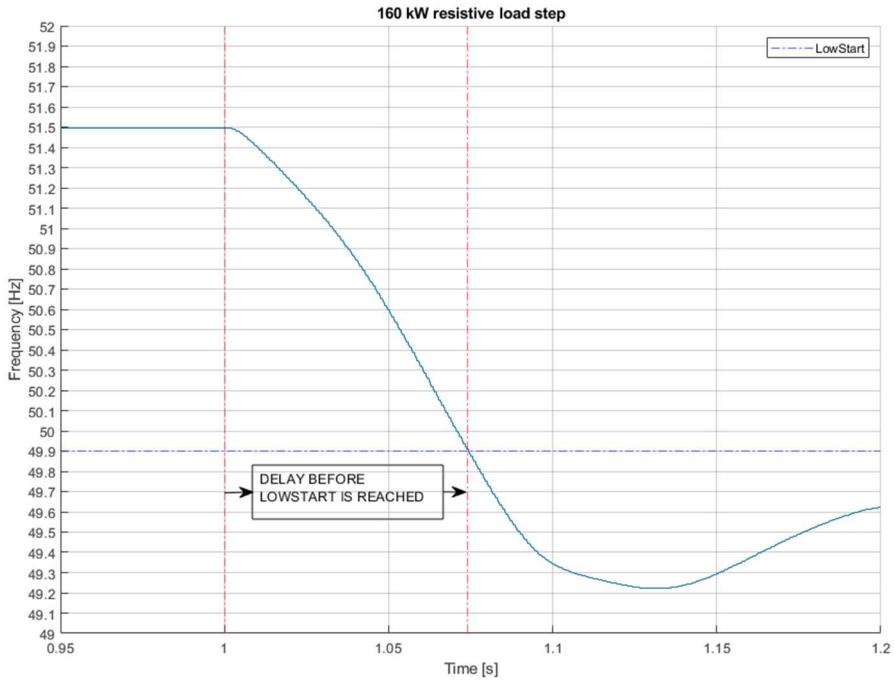

Figure 4-17: Linear droop "delay" as seen from a 160 kW resistive load step when the system frequency is 51.5 Hz before the step and LowStart is set to 49.9 Hz.

In addition to the dead band parameters (*RocofLowStart*), maximum ROCOF values (*RocofLowMax*) and power thresholds (*MaxRocofTerm*), the ROCOF-based power command has a configurable rate limited response, which is configured by the parameters *FallingRampRate* and *RisingRampRate*. This way, a more restrained and stable response is achieved, as the frequency, and consequently the power, tend to oscillate after a fast active power injection, as seen with the more aggressive linear droop parameters in Figure 4-16. Though the *RisingRampRate* parameter should not be limited too much, as then the response speed would diminish, which is the main advantage of the method. *FallingRampRate* setting mainly depends on the feeding generators response speed. If the parameter is set too high, and the power command is let to decrease quickly after the frequency has started recovering, the generator may still be ramping up which would cause the frequency to drop again. On the other hand, setting the parameter too low will decrease the effectiveness of the regulation method as excessive energy would be utilized in the response.

The ROCOF-control performance in load steps is shown in Figures 4-18 and 4-19, which is now compared to the linear droop method, instead of the no regulation responses. The 100 to 200 kW load step is left out of the tests as the performance is very similar to the 100 kW load step. The control parameters in the figures are as shown in Table 4-2. First, the ROCOF-control's frequency droop is parametrized as in linear droop 1 case. With *MaxDRPower* set to 100 % and *MaxRocofTerm* set to 50 %, it means that the ROCOF-based response can only contribute to 50 % (100 kW) of regulation power and the rest (100 kW) are controlled by the frequency droop, if required. The *RocofLowStart* and *RocofLowMax* values are first set based on the ROCOF values seen in the load steps with no regulation (Figure 4-7). In the context of this thesis and the small-scale power system being tested, there are no reference values for maximum ROCOF, so the parameters are chosen using trial and error. However, if this control method would be utilized in a larger scale power system with more inertia, these parameters could be more easily selected analytically (see subsection 3.2.1, ROCOF withstand capabilities, inertia estimation). Additionally, if the worst-case scenario load imbalance in the power system can be estimated, it is possible to calculate the maximum ROCOF using Equation (3-5). This estimate could then be used as a reference for the *RocofLowMax* parameter. Moreover, as the system only consists of a single generating unit, the genset performance class target values could provide some reference, as discussed in subsection 3.2.1.

Table 4-2: Control parameters for the frequency regulation performance demonstration in Figures 4-18 – 4-20.

Parameter	**Linear droop 1**	**Linear droop 2**	**ROCOF-control**	**ROCOF-control 2 (Fig. 4-20)**	**ROCOF-control 3 (Fig. 4-20)**
NominalFrequency (Hz)	50	50	50	50	50
LowStart (Hz)	49.9	49.9	49.9	49.9	49.9
LowMax (Hz)	48.0	49.5	48.0	49.0	49.0
RampStart (%)	0	0	0	0	0
MaxDRPower (%)	100	60	100	100	100
RocofLowStart (Hz/s)	-		-3.5	-1.5	-1.5
RocofLowMax (Hz/s)	-		-30	15	-20
MaxRocofTerm (%)	-		50	50	60
FallingRampRate (%/s)	-		-100	-25	-Inf
RisingRampRate (%/s)	-		Inf	Inf	Inf

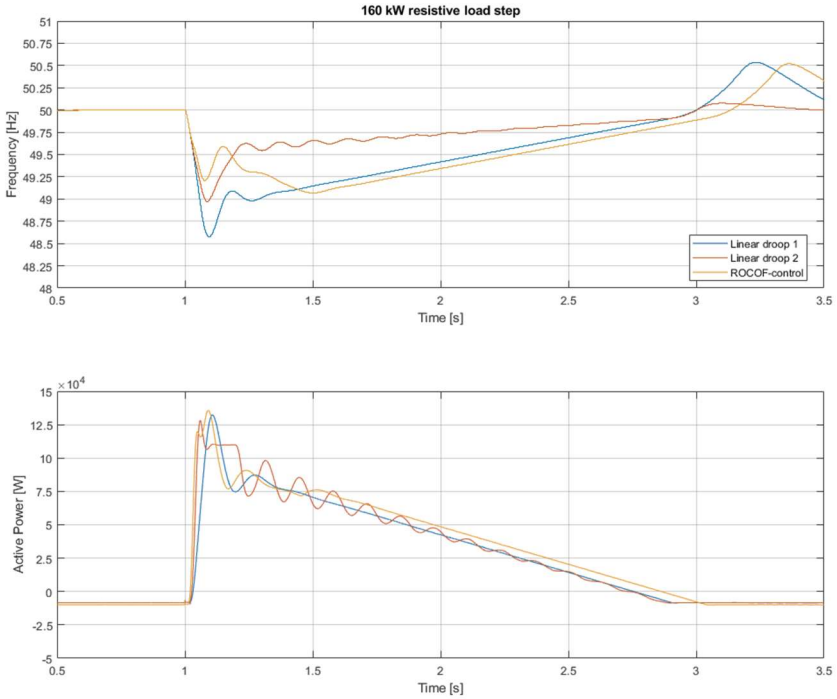

Figure 4-18: System frequency and active power from the UPS after a 160 kW resistive load step, comparison between linear droop and ROCOF-control.

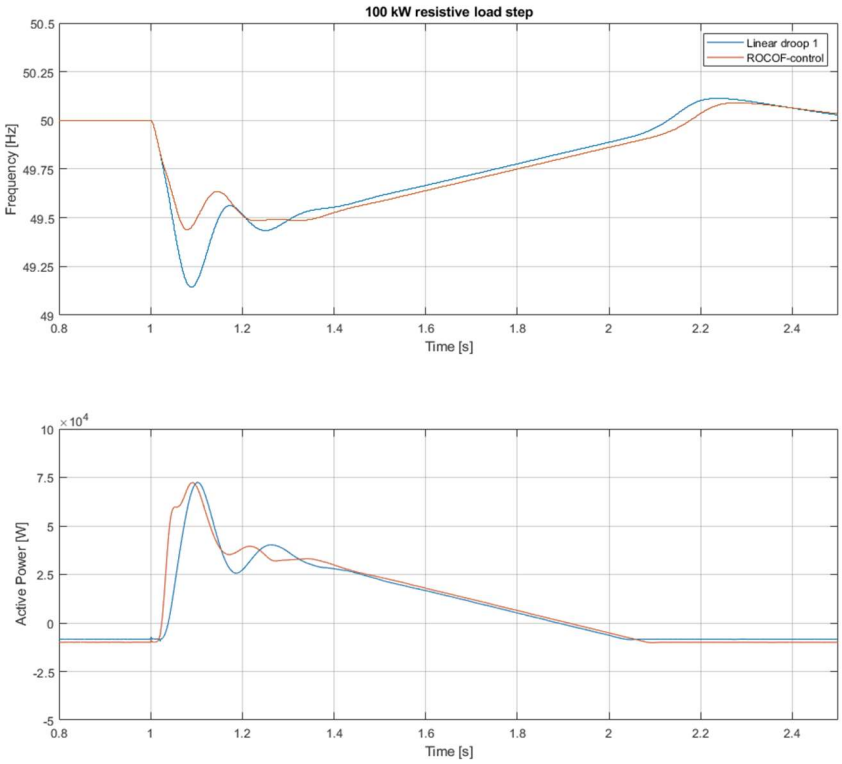

Figure 4-19: System frequency and active power from the UPS after a 100 kW resistive load step, comparison between linear droop and ROCOF-control.

As can be seen from the load step performances in Figures 4-18 and 4-19, the ROCOF-control method has some advantages when compared to the linear droop method. The ROCOF-control reacts faster to the load step: for example, in the 100 kW step, the ROCOF-control has reached 50 kW of regulation power approximately 32 ms earlier than the linear droop method. Additionally, the frequency nadir increased by 0.3 Hz. The figures also show that even though the performance increased, the amount of power used for regulation is nearly the same as with linear droop. The best way to show the advantage of the ROCOF-control method is shown in Figure 4-20, where the system frequency before the load step is above nominal. The ROCOF-control starts almost immediately limiting the ROCOF, and especially with the more aggressive parameters in *ROCOF-control 2*, a much steadier response is achieved as the frequency settles to 50 Hz without much undershoot. However, it should be noted that the *ROCOF-control 2* case has *FallingRampRate* parameter set to relatively low value (25 %/s), which could introduce problems, if the power imbalance recovers faster than normal, for example due to increased generation or decreased load. This highlights the importance of correct parameter settings for the control and the fact that the parameters are highly dependent on the nature of the generation capacity. Moreover, *ROCOF-control 3* demonstrates that

the *FallingRampRate* parameter is not necessarily required, and sufficient performance can still be achieved.

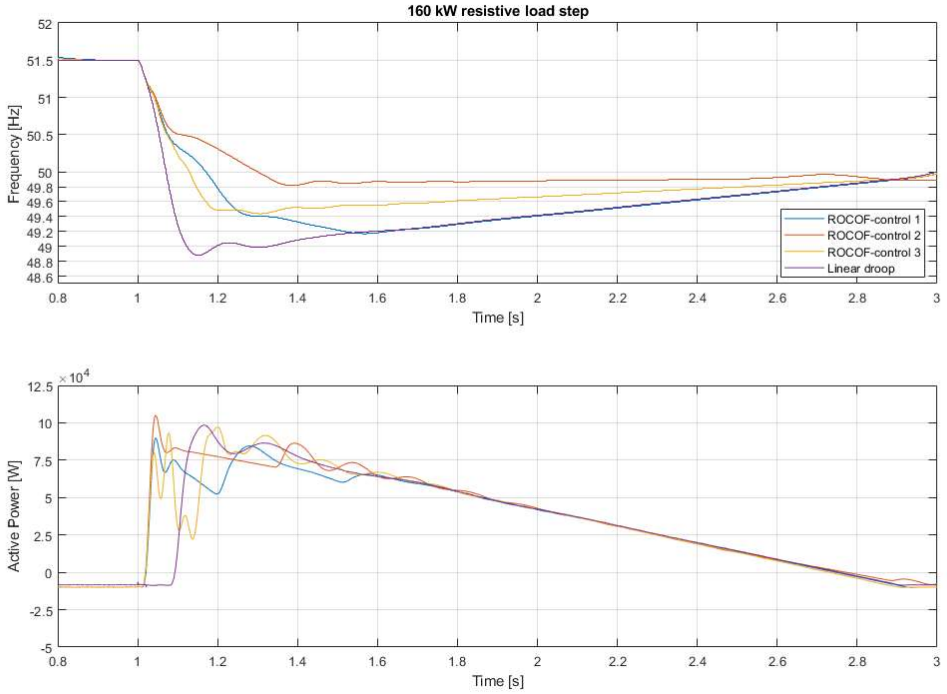

Figure 4-20: System frequency and active power from the UPS after a 160 kW resistive load step, comparison between linear droop and ROCOF-control configurations. Abnormal system frequency before the load step.

4.4.3 Piecewise linear-elliptic droop

The linear droop method works effectively, even in fast frequency deviations, and implementing a secondary ROCOF-based response improved it slightly more. These two methods are chosen for the implementation part of this thesis as they are relatively easy to implement and seem to achieve good performance. As a final consideration, a slightly advanced non-linear droop method is tested in the simulation environment.

The piecewise linear-elliptic (PLE) droop control was introduced in [77], and a similar control scheme is now implemented into the simulation model. The PLE droop curve shown in Figure 4-21 has a linear region near the nominal frequency and outside of that, the power trajectory is elliptic. The elliptic up-regulation power response of the PLE droop can be formulated as:

$$P_{PLE} = \sqrt{\frac{(f_n - f_{LowMax})^2 - (f - f_{LowM\quad})^2}{R^2}}, \qquad (4\text{-}2)$$

where f_n is the nominal frequency, f_{LowMax} is the minimum frequency, *f* is the measured frequency and *R* is the droop coefficient. The droop coefficient *R* represents the amount of power used for regulation as a function of the frequency. Thus, it can be chosen based on the maximum frequency deviation (f_{LowMax}) and the desired regulation power at that point. Decreasing the value of *R* leads to a more aggressive response (more injected power) but may also lead to instability.

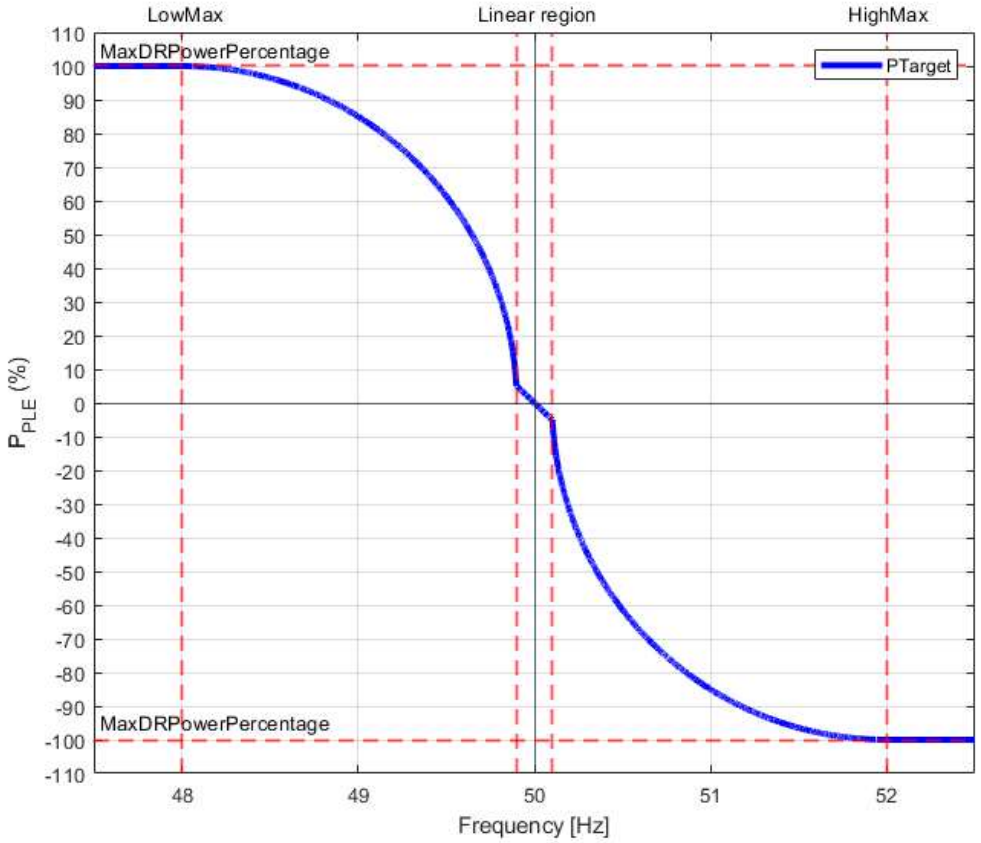

Figure 4-21: The implemented PLE droop curve.

The performance of the PLE-droop is demonstrated in Figure 4-22 where the system frequency response to a 160 kW load step is shown. As seen from the figure, the elliptic trajectory results in a more aggressive initial power response when compared to linear droop and as result, the frequency nadir is improved by approx. 0.5 Hz. Additionally, the recovery period after the initial frequency drop is superior with PLE, as the frequency is well above of those in the linear droop or ROCOF-control cases. In Figure 4-22, the PLE is configured with $f_{LowMax} = 48.0$ Hz and $R = 0.0186$. The linear region is between nominal frequency and 49.85 Hz with droop coefficient set to 0.022. These parameters seemed to give an effective response without leading to instability. The values indicate

that the UPS regulates at its maximum (approximately) when the frequency has decreased to 48.0 Hz.

As discussed in [77], decreasing the linear region makes the response faster and this will result in better dynamic performance. However, this might introduce problems when dealing with smaller deviations as the control might react too abruptly. Also, a too small linear region resulted in an unstable recovery, when the frequency approached its nominal value.

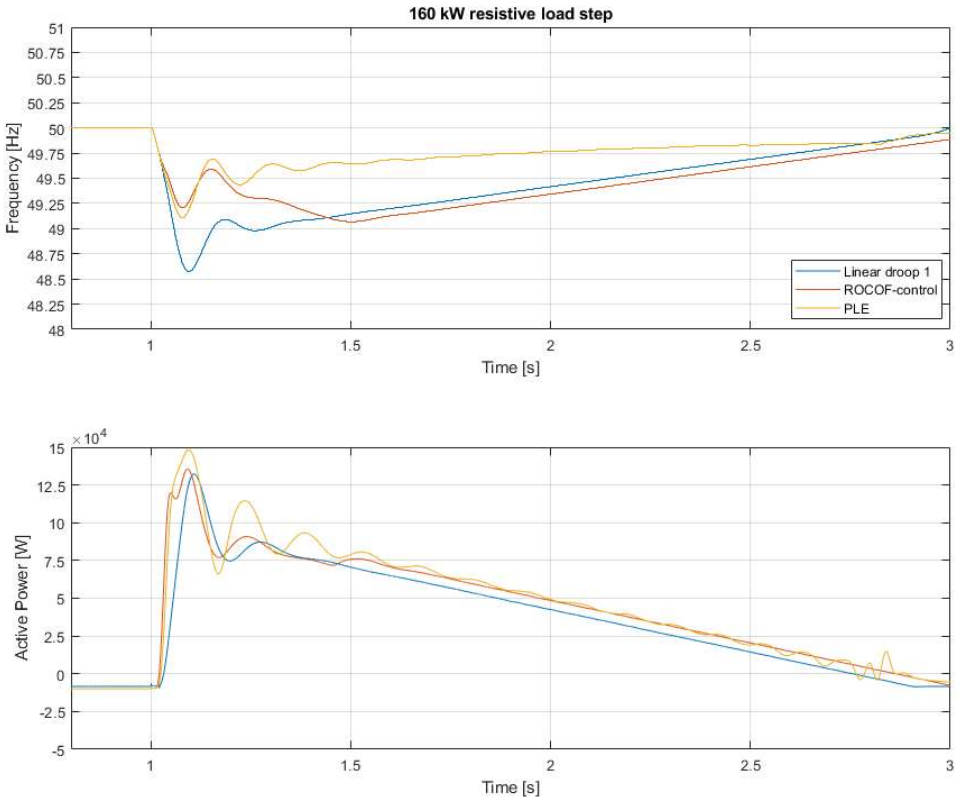

Figure 4-22: System frequency and active power from the UPS after a 160 kW resistive load step, comparison between linear droop, ROCOF-control and PLE-droop.

5. IMPLEMENTATION OF THE FREQUENCY REGULATION AND LABORATORY TESTING

Now that the frequency regulation algorithms have been designed and evaluated in a simulation environment, they are implemented for an Eaton 200 kW 93PM double-conversion UPS, shown in Figure 5-1a. In this chapter, the firmware implementation of the frequency regulation algorithm is described, and the algorithm is tested in a laboratory environment. Only the linear droop and ROCOF-control methods are tested in this case study with few different parametrizations.

5.1 Implementing the algorithm into a UPS device

The 93PM is a modular UPS that consists of multiple (four in this case) power modules (UPMs) that each has its own control firmware. However, the frequency regulation is implemented into the system-wide controller, machine control unit (MCU), that communicates through CAN-bus[4] to the UPMs. This means that the calculated power command sent through CAN for each UPM is identical, and the load is shared evenly between the 50 kW UPMs. After the UPM receives the power command, it sets the power target for the battery converter, which then controls its output power towards the target. Additionally, the demand response scheme includes different protection functionalities, for example checking that the battery capacity is enough for the regulation to continue and checking that the UPS is operating normally.

The implementation of the fast frequency regulation algorithm is done by using the pre-existing *UPSaaR* control firmware for the 93PM as a platform and adding a separate control mode for the ROCOF-control. Additionally, the sub-cycle frequency measurement is added into the *dq*-PLL in the UPS MCU firmware. Originally in the 93PM products, the *UPSaaR* functions have been implemented into a 100 ms periodic task, which essentially means that the power command could only be updated every 100 ms. This renders the faster method useless, as there would be no benefit with the faster frequency measurement, if the sampling is done every 100 ms. This was also verified by simulation; the 100 ms sampling interval for the regulation algorithm was not fast enough in the load steps as the ROCOF values are so high. Additionally, the original/pre-existing 100 ms *UPSaaR* droop-mode was tested with the laboratory setup and the results are discussed

[4] CAN-bus (Controller Area Network) is a common communication network protocol used in various applications, for example vehicles, industrial automation etc.

later in Section 5.3. Thereby, the entirety of the *UPSaaR* control platform was reimplemented into a faster control loop that is run every 5 ms. The 5 ms sampling interval seemed to be fast enough for the intended purposes.

As discussed in Chapter 4, the regulation algorithm has a lot of different parameters that significantly affect the performance of the system. To make the practical testing with different parameters easier, the configurable parameters are implemented into electrically erasable programmable read-only memory (EEPROM). This allows the user to change the relevant control parameters on the fly via a service tool designed for the UPS that is capable of reading and writing these EEPROMs.

5.2 Test setup specifications

The performance of the frequency regulation is tested in a laboratory environment where an isolated diesel generator fed test network is constructed. The schematic diagram of the test network is shown in Figure 5-1b. The generator G1, shown in Figure 5-2, is a 250 kVA AGCO Power AG250 diesel generating set, and the UPS1 is the previously described 200 kW Eaton 93PM. The UPS has two sets of VRLA battery packs connected to it. There are also two different sets of resistive load banks: LOAD1 is connected in parallel with the UPS1 i.e., in the input side of the UPS. LOAD2 is connected to the output of the UPS and it can provide up to 100 kW of resistive load.

The input voltage and current of the UPS are measured with a digital oscilloscope and the frequency of the grid is separately calculated with MATLAB after the tests. During the tests, the UPS is set to operate in double conversion mode, i.e., the input voltage is rectified and inverted back to form the output voltage. One of the requirements for frequency regulation with UPS is that the protection of the critical load should not be compromised, and the UPS should be able to operate normally. Even though the test setup does not have UPS output measurements, the continuity of UPS operation can be verified by checking the logged data and the active alarms in the display of the UPS, which will indicate possible faulty situations, e.g., DC link overvoltages or output undervoltages.

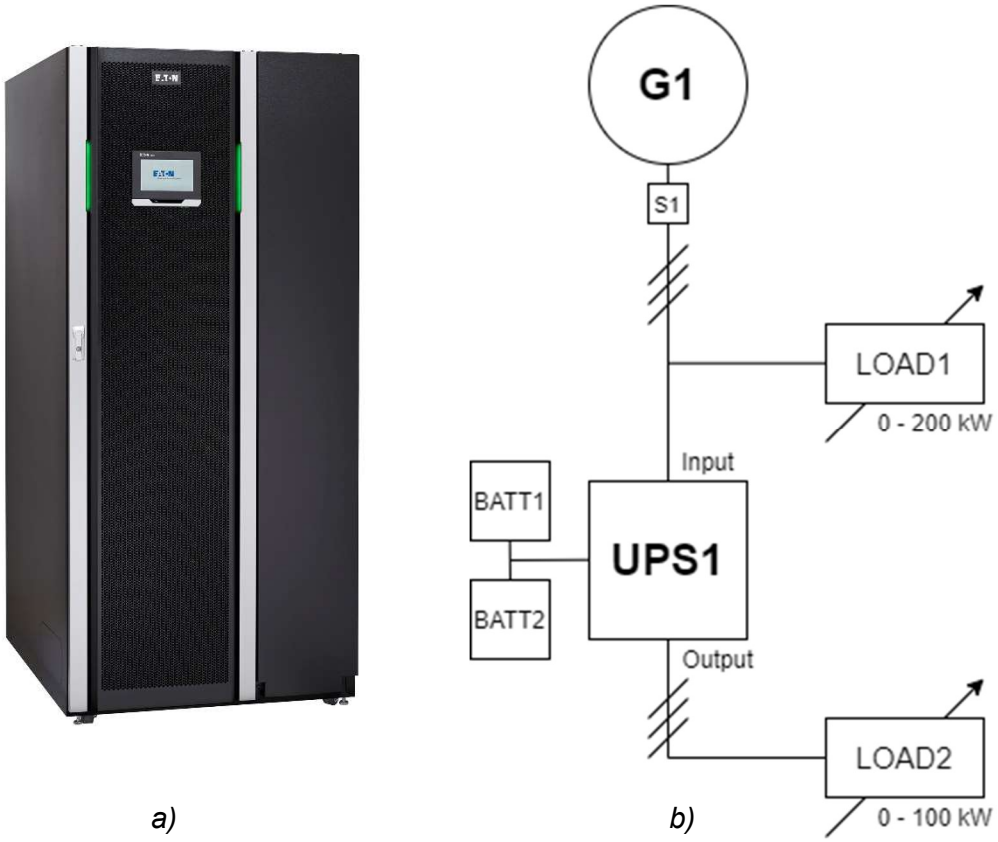

Figure 5-1: a) Eaton 93PM UPS [78], b) Schematic diagram of the test laboratory setup.

Figure 5-2: AGCO Power AG250 diesel generator. [79]

5.3 Measurement results with different control modes and parameters

As with the simulations, the first tests are done with the frequency regulation disabled to benchmark the generator's performance in different-sized load steps. It should be noted that the generator is operated in speed droop mode with ~3 % droop. This means that the no-load system frequency is about 51.5 Hz. Figure 5-3 shows the system frequency, ROCOF and voltage d-component during 50 kW, 100 kW and 160 kW resistive load steps. The performance is not exactly as in the simulated system, but the deviations are in the same order of magnitude. The 50 kW step is small enough so that the frequency stays within the droop range, i.e., it does not deviate below 50 Hz. The 160 kW step was found to be the load step limit for the generator with the used settings, as any bigger load step would cause the generator protection system to trip.

The next step was to test the *UPSaaR* frequency droop with the default, slower control, i.e., 100 ms control loop and slower frequency measurement. However, the UPS was not able to do any reasonable demand response actions with the slower control in this kind of low-inertia microgrid and thus it was deemed useless.

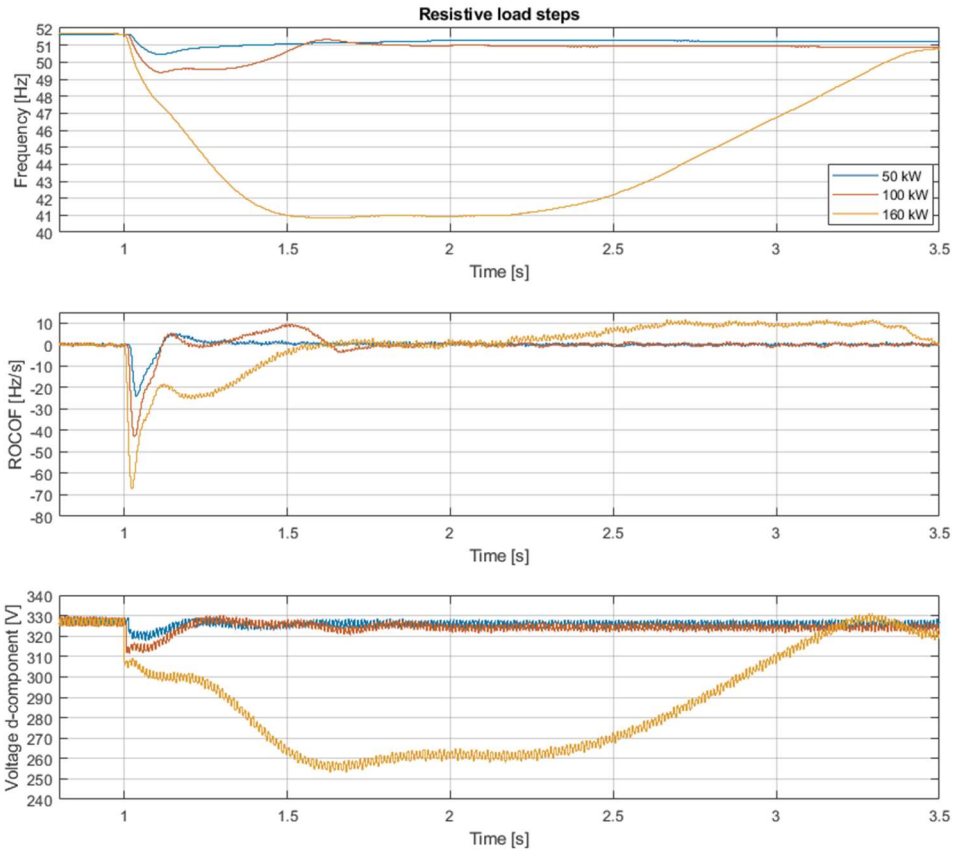

Figure 5-3: The system frequency, ROCOF and voltage d-component during 50, 100 and 160 kW resistive load steps. Frequency regulation disabled.

Next, the droop-mode and ROCOF-control are tested with the sub-cycle frequency measurement and the faster, 5 ms control loop. Even though the frequency is well above 50 Hz before the load step, the *LowStart* parameter is set to 49.9 Hz, as it realistically cannot be set above 50 Hz to prevent unnecessary demand response. After a couple of trial runs, it was found that the optimal setting for *LowMax* was 48.0 Hz as setting the parameter any higher would result in an unstable response.

Parametrizing the ROCOF-control is slightly more intricate if the control needs to be more aggressive, as the response is easily unstable. However, setting the *RocofLowStart* to 3.5 Hz/s, *RocofLowMax* to 100 Hz/s and limiting the ROCOF-based power response falling ramp rate to 100%/s seemed to give a slightly improved response when compared to the linear droop method.

Figure 5-4 shows the performance of the two control modes compared to no regulation in a 100 kW resistive load step. The linear droop method improved the frequency nadir by 0.29 Hz and the ROCOF-control by 0.72 Hz. The power responses in both cases are two short bursts of power injections. The dynamics of the control delays, charger performances etc. can clearly be detected. For example, at around t = 1.2 s, the ROCOF-control regulation power has decreased to zero, even though the ROCOF is clearly negative. However, the delay is short enough (< 50 ms) that the control remains stable and a fast response can be achieved. The 100 kW load step was just small enough that the ROCOF-control achieved to keep the frequency above 50 Hz at all times, and therefore the entirety of the power response is based on ROCOF.

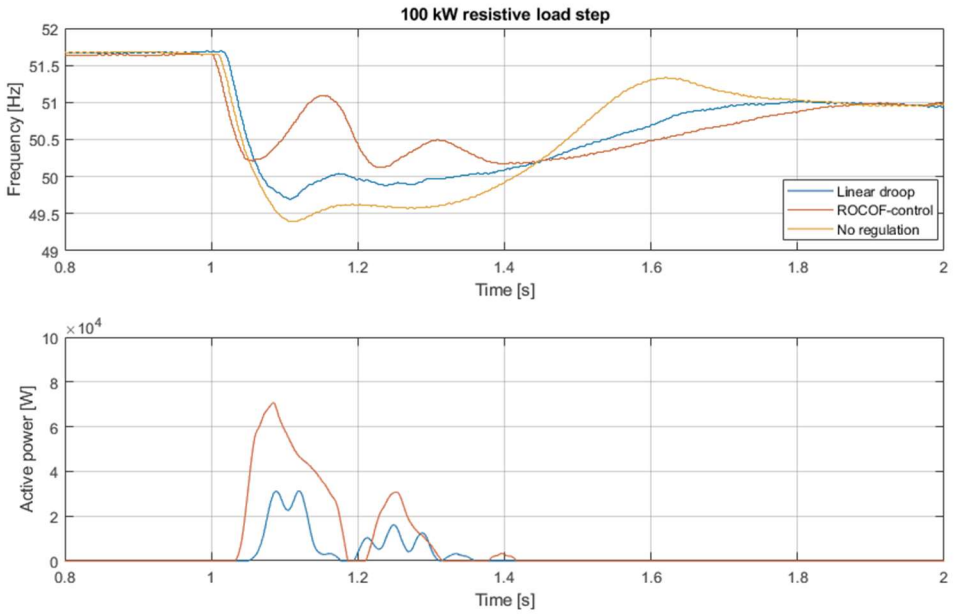

Figure 5-4: System frequency and UPS regulation power after a 100 kW resistive load step, comparison between linear droop, ROCOF-control and no regulation.

A more dramatic effect of the frequency regulation control can be seen in Figure 5-5, where the performances of the control modes are compared to no regulation in a 160 kW load step. The frequency nadir improved by approx. 8 Hz, and the frequency settled around 1 s faster. Additionally, the voltage deviation was reduced significantly. However, the ROCOF-control does not show that much advantage over the linear droop as the frequency nadir improved only by 0.04 Hz. The ROCOF-control reacts approximately 40 ms faster than the linear droop, but in terms of frequency, the improvement is insignificant. The ROCOF-control could not be configured to be more aggressive as it led to unstable responses, but there might be possibility to enhance the response by decreasing the *FallingRampRate* parameter to match the performance of the genset.

As stated earlier, the diesel generator's load step acceptance limit was found to be 160 kW without supplementary regulation. However, with the added frequency support from the UPS, the power system can undergo even bigger load steps, up to the kW-rating of the generator. Figure 5-6 shows the system frequency and UPS regulation power during a 200 kW resistive load step. Finally, in Figure 5-7, the performance of the regulation is demonstrated in a more realistic case, where the UPS has 100 kW (50 %) of load and the feeding grid undergoes a 100 kW load step. In this case, the UPS does not feed power back to the input as it only takes power from the batteries to support the critical load, thus reducing the power imbalance experienced by the generator.

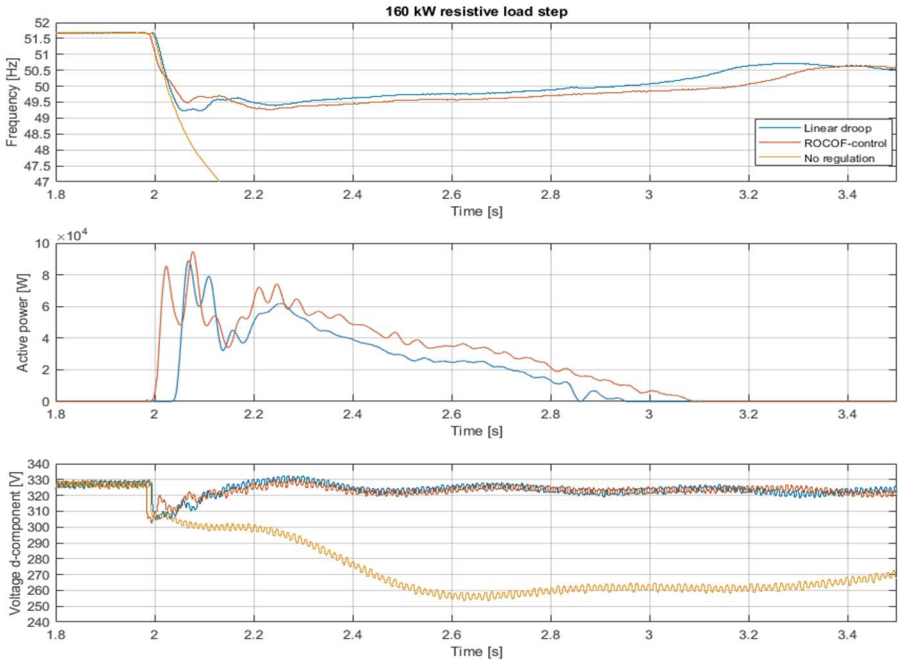

Figure 5-5: System frequency and UPS regulation power after a 160 kW resistive load step, comparison between linear droop, ROCOF-control and no regulation.

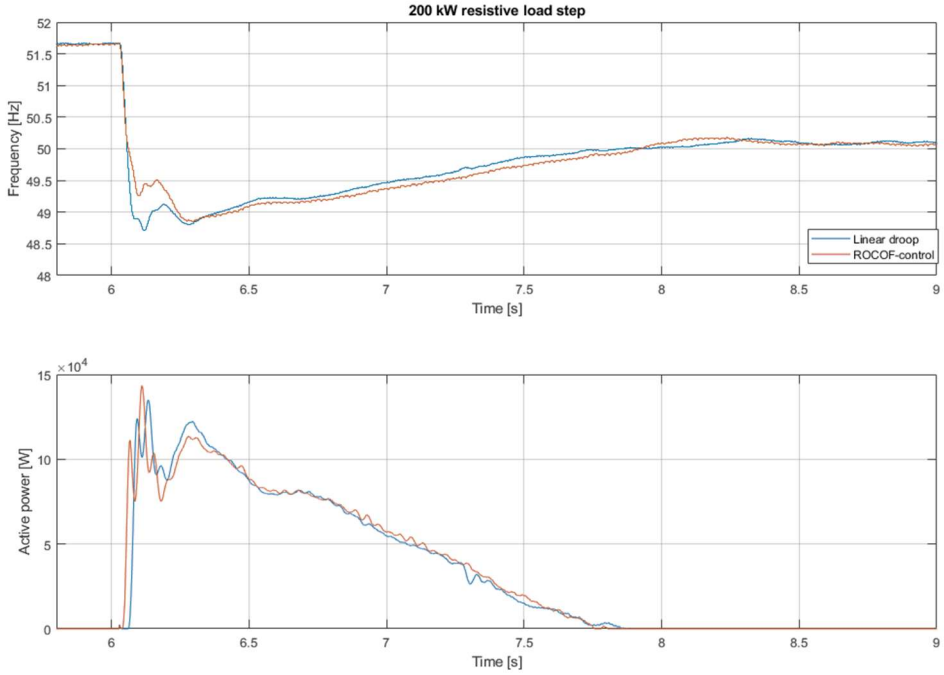

Figure 5-6: System frequency and UPS regulation power after a 200 kW resistive load step, comparison between linear droop and ROCOF-control

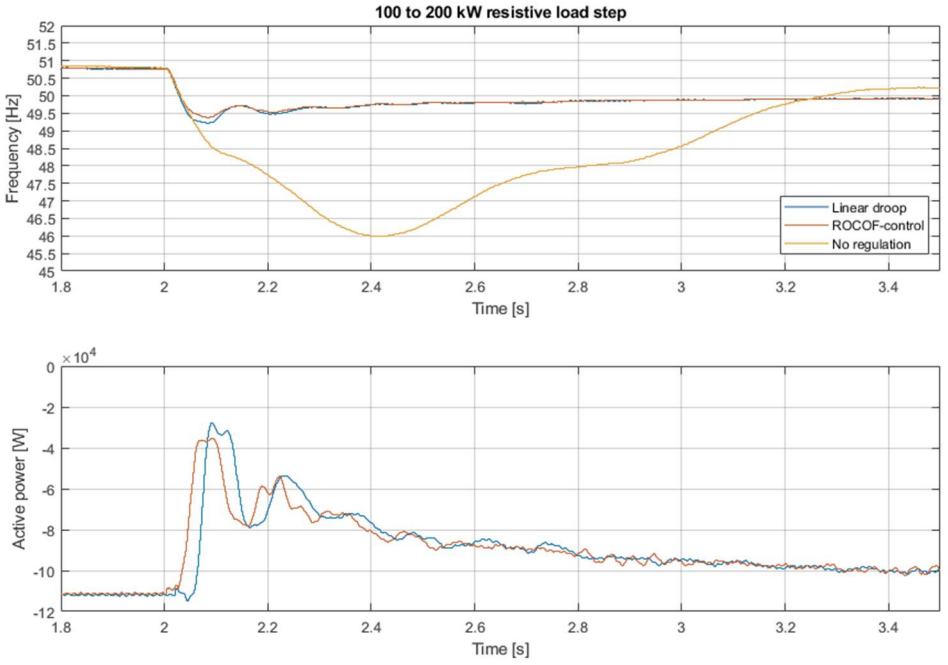

Figure 5-7 System frequency and UPS regulation power after a 100 kW resistive load step with 100 kW UPS base load, comparison between linear droop, ROCOF-control and no regulation.

6. SUMMARY AND CONCLUSION

The objective for this thesis was to study the capability of UPS devices in providing frequency regulation in the context of low-inertia islanded/isolated microgrids. The background for this type of unusual UPS application comes from the Eaton EnergyAware and UPS-as-a-Reserve features that enable the data center UPSs to provide frequency regulation services to the feeding grid. The EnergyAware UPS is intended for utility-scale electric grids and the frequency containment reserve markets. In this context, the control problem is relatively slow when compared to the possibilities that state-of-the-art power electronics and energy storages provide. The utility grid generation capacity is primarily based on large synchronous generators that bring inertia to the system, which makes the frequency deviations less severe. However, as the system inertia decreases, for example due to increasing amount of inertialess renewable energy sources, the frequency deviations get faster (i.e., higher ROCOF) and bigger. To combat this problem, different frequency regulation solutions have been studied and implemented, for example fast frequency reserves (FFR) and virtual inertia methods.

As a continuity to these solutions and the EnergyAware UPS, the frequency stability problem due to low-inertia was studied in the context of an isolated power system where the generation capacity is provided by a back-up generator. This kind of system could be used when a data center with UPS systems is temporarily islanded from the main grid. Alternatively, the microgrid could also be intentionally isolated with its own generation capacity based on renewables and gensets. Regardless, the data center UPSs can now be used to provide frequency support in the low-inertia grid and to help the genset(s) survive larger load steps.

The frequency regulation methods for the UPS were first studied in a simulation environment utilizing MATLAB Simulink. A simple power system consisting of a diesel genset and a double-conversion UPS was constructed, where the UPS model was represented by an active rectifier circuit for simplification. The control algorithms utilize the frequency measurement from the input voltage of the UPS and calculate appropriate power responses to regulate the frequency. The power response is used to control the power flow from the UPS battery, either to supply the UPS load or to feed power back to the grid. In addition to designing the regulation methods, a sub-cycle frequency measurement was implemented into the PLL to achieve faster tracking of the input frequency.

A few control modes were tested: linear droop, virtual inertia or ROCOF-control and PLE-droop. These methods were tested by simulating resistive load steps to the UPS input-side grid, which produced extreme frequency deviations. All the control modes improved the load acceptance and frequency nadir significantly, when compared to the case where frequency regulation was disabled. Additionally, the voltage drop of the generator was also greatly reduced as the generator's voltage regulator did not require under frequency roll-off. For example, in the 100 kW load step, the linear droop improved the frequency nadir by over 2 Hz. The ROCOF-control had some additional benefits to it by making the response a bit faster and a slight improvement (0.3 Hz in the 100 kW step) in the frequency nadir was seen. However, configuring the parameters for ROCOF-control was found to be challenging, and the control mode was prone to instability. The PLE droop performance was quite promising: the initial frequency drop was very similar to the ROCOF-control, which indicates that the power response speed was equivalent. Additionally, the recovery period after the initial drop was superior. The advantage of this method is that a better response is achieved without needing the ROCOF measurement, which can be sensitive to all kinds of disturbances. All in all, it is concluded that the sub-cycle frequency measurement enables the UPS device to achieve fast enough responses to react to the power imbalances in the low-inertia grid (regardless of the control method).

To verify the performance of the control methods, a laboratory test setup was constructed with a 250 kVA diesel genset feeding a 200 kW Eaton 93PM double-conversion UPS with EnergyAware capabilities. As a reference test, the genset was subjected to relatively large resistive load steps to benchmark the performance of the generator. The genset could accept a maximum 160 kW load step without tripping its underspeed protection and in this case, the frequency nadir was approximately 41 Hz with the initial maximum ROCOF around 65 Hz/s. These values seem unreasonable in the context of conventional power systems, but it should be noted that this type of genset is not designed to accept load steps this big. However, as seen with the simulations, supporting the genset with the UPS frequency regulation methods, the load steps could be achieved within reasonable frequency deviations. A brief summary of the measurement results is presented in Table 6-1. When looking at the results from the 160 kW load step, it is clear that the ROCOF-control does not have a significant advantage over the linear droop. However, some added benefit can be seen in the 100 kW load step results, as the nadir and the mean value of the frequency are improved. It should be noted that as seen with the simulations, the parametrizing of the ROCOF-control was challenging, and the method was prone to instability.

Table 6-1: Summary of the UPS frequency regulation method performances from the laboratory testing measurements.

Attribute	**No regulation[1]**	**Linear droop[1]**	**ROCOF-control[1]**
Frequency nadir (Hz)	49.4, 40.8	49.7, 49.2	50.1[3], 49.3
Max ROCOF[2] (Hz/s)	-40.5, -62.5	-42.2, -58.2	-39.5, -50.0
Mean frequency[4] (Hz)	49.9, 43.8	50.2, 49.8	50.5 ,49.7
Voltage drop (%)	4.1, 22.0	4.6, 6.2	4.3, 6.0
Peak regulation power (kW)	-	31.2, 88.7	70.7, 94.6
Active time (ms)[5]	-	312, 920	385, 1125

1 *Values from 100 kW and 160 kW load steps, respectively.* **2** *Maximum initial ROCOF, no averaging.* **3** *Genset in droop mode, steady-state frequency above 50 Hz, thus nadir could be maintained above 50 Hz.* **4** *The average (mean) frequency from the whole event.* **5** *Represents the total time the UPS regulation was active.*

Overall, the simulations and the laboratory testing were successful, and it was clearly demonstrated that the Eaton EnergyAware 93PM UPS is capable of providing frequency support in extremely low-inertia grids. From the two control modes tested, linear droop was overall better as it achieved very similar results compared to the ROCOF-control with less complexity. The linear droop method was much easier to parametrize to be stable and does not require sensitive ROCOF measurements. However, utilizing the system ROCOF as a control input is something that could be better suited for a larger scale microgrid, as suggested by virtual inertia studies. Additionally, adaptive methods as discussed in subsection 3.2.2 would be an interesting topic to research in terms of these kinds of low-inertia systems.

Lastly, as discussed before, these control methods are very dependent on accurate and fast frequency measurements. Therefore, as a suggestion for future research, alternative

frequency estimation methods should be considered, as the digital dq-PLL based frequency estimation utilized in this work was sub-optimal. Furthermore, these low-inertia frequency regulation methods should also be tested for ‘down-regulation’ and load rejection capabilities, which would require for example Li-ion batteries to enable higher power charging. Utilization of supercapacitors as an energy storage solution for this kind of fast regulation could also be worth considering, as the activation times shown in Table 6-1 were relatively short and only quick power peaks were required.

SOURCES

[1] Zou C, Zhao Q, Zhang G, Xiong B. Energy revolution: From a fossil energy era to a new energy era. Natural Gas Industry B, 2016, Vol 3, pp. 1 – 11.

[2] Ørum E, Haarla L, Kuivaniemi M, Laasonen M, Jerkø A, Stenkløv I, et al. Future System Inertia 2. ENTSO-E Report. Brussels, Belgium, 2018. Available: https://www.fingrid.fi/globalassets/dokumentit/fi/yhtio/tki-toiminta/raportit/nordic-report-future-system-inertia2_vfinal.pdf (accessed Feb 2021).

[3] Tamrakar U, Shrestha D, Maharjan M, Bhattarai B, Hansen T, Tonkoski R. Virtual Inertia: Current Trends and Future Directions, Applied sciences, 2017, Vol. 7, Iss. (7): p. 654–.

[4] Tielens P, Van Hertem D. The relevance of inertia in power systems. Renewable & sustainable energy reviews, 2016, Vol. 55, pp. 999–1009.

[5] Kundur P. Power system stability and control. McGraw-Hill Education, 1st edition Jan 1994, pp. 128 – 139.

[6] Lasseter B. Microgrids [distributed power generation]. In: 2001 IEEE Power Engineering Society Winter Meeting Conference Proceedings (Cat No01CH37194). IEEE; 2001, Vol. 1, p. 146 – 149.

[7] Marnay C, Robio F., Siddiqui A. Shape of the microgrid. In: 2001 IEEE Power Engineering Society Winter Meeting Conference Proceedings (Cat No01CH37194). IEEE; 2001, Vol.1, p. 150 – 153.

[8] Stadler M, Cardoso G, Mashayekh S, Forget T, DeForest N, Agarwal A, et al. Value streams in microgrids: A literature review. Applied energy. 2016, Vol. 162, Iss. (C): pp. 980 – 989.

[9] Beck H-P, Hesse R. Virtual synchronous machine. In: 2007 9th International Conference on Electrical Power Quality and Utilisation, EPQU, 2007.

[10] Alaperä I, Honkapuro S, Paananen J. Data centers as a source of dynamic flexibility in smart girds, Applied energy, 2018, Vol. 229, pp. 69 – 79.

[11] I. Alaperä, J. Paananen, K. Dalen and S. Honkapuro, Fast frequency response from a UPS system of a data center, background, and pilot results. 2019 16th International Conference on the European Energy Market (EEM), Ljubljana, Slovenia, 2019, pp. 1 – 5.

[12] Eaton Corporation. Eaton EnergyAware UPS, Website, Available: https://www.eaton.com/us/en-us/products/backup-power-ups-surge-it-power-distribution/backup-power-ups/energyaware-ups.html (accessed Feb 2021).

[13] Hansson M. Virtual Inertia from UPS Systems, M.Sc. thesis, Lappeenranta University of Technology, Lappeenranta, 2019.

[14] Energiavirasto. Sähkö- ja maakaasuverkkotoiminnan kehittäminen, Website, Available: https://energiavirasto.fi/verkkotoiminnan-kehittaminen (accessed Mar 2020).

[15] Geng H, Geng H. Data center handbook. 1st edition, Hoboken, New Jersey USA: John Wiley & Sons Inc.; 2015.

[16] Davies TC. Which UPS is right for the job: Static, rotary or hybrid? Consulting-specifying engineer, 2006-12, Vol. 40, Iss. (6), p. 56.

[17] Bekiarov SB, Emadi A. Uninterruptible power supplies: Classification, operation, dynamics, and control. In: Conference Proceedings - IEEE Applied Power Electronics Conference and Exposition – APEC, 2002, p. 597 – 604.

[18] Aamir M, Ahmed Kalwar K, Mekhilef S. Review: Uninterruptible Power Supply (UPS) system, Renewable & sustainable energy reviews, 2016, Vol. 58, pp. 1395 – 1410.

[19] Krishnan R, Srinivasan S. Topologies for uninterruptible power supplies. In: ISIE '93 - Budapest: IEEE International Symposium on Industrial Electronics Conference Proceedings, IEEE, 1993. pp. 122 – 127.

[20] Racine M., Parham J., Rashid M. An overview of uninterruptible power supplies. In: Proceedings of the 37th Annual North American Power Symposium, 2005. IEEE; 2005. pp. 159–164.

[21] Rashid M, Rashid MH. Power electronics handbook. 4th edition, Oxford, England: Butterworth-Heinemann, 2018, pp. 385 – 416, pp. 641 – 658.

[22] Eaton Corporation. Eaton 93PM UPS 30-250kVA User's and installation guide, P-164000249, Revision 006, Espoo 2018, p. 20.

[23] Rodriguez J., Dixon J., Espinoza J., Pontt J, Lezana P. PWM regenerative rectifiers: state of the art, IEEE transactions on industrial electronics (1982), 2005, Vol. 52, Iss. (1), pp. 5 – 22.

[24] Blaabjerg F. Control of power electronic converters and systems, Volume 2. London, United Kingdom, Academic Press, 2018, pp. 3 – 52.

[25] IEC 61000-3-12 Electromagnetic compatibility (EMC) - Part 3-12: Limits - Limits for hamonic currents produced by equipment connected to public low-voltage systems with input current > 16 A and ≤ 75 A per phase, IEC Standard, 2011.

[26] IEC 62040-3 Uninterruptible power systems (UPS) - Part 3: Method of specifying the performance and test requirements, IEC Standard, 2011.

[27] Sharkh SM. Power electronic converters for microgrids. Singapore, Wiley-IEEE Press, 2014, pp. 14 – 15.

[28] Escobar G, Leyva-Ramos J, Carrasco J., Galvan E, Portillo R., Prats M., et al. Modeling of a three level converter used in a synchronous rectifier application. In: 2004 IEEE 35th Annual Power Electronics Specialists Conference (IEEE Cat No04CH37551), Piscataway NJ, IEEE, 2004, Vol. 6, p. 4306 – 4311.

[29] Ventosa-Cutillas A, Montero-Robina P, Umbría F, Cuesta F, Gordillo F. Integrated Control and Modulation for Three-Level NPC Rectifiers. Energies (Basel), 2019, Vol.12, Iss. (9), p. 1641.

[30] Freijedo FD, Doval-Gandoy J, Lopez O, Martinez-Penalver C, Yepes AG, Fernandez-Comesana P, et al. Grid-synchronization methods for power converters, In: 2009 35th Annual Conference of IEEE Industrial Electronics, IEEE, 2009, p. 522 – 529.

[31] Teodorescu R, Rodríguez P, Liserre M. Grid converters for photovoltaic and wind power systems, Chichester, West Sussex, Wiley, 2010, pp. 169 – 204.

[32] Ali Z, Christofides N, Hadjidemetriou L, Kyriakides E, Yang Y, Blaabjerg F. Three-phase phase-locked loop synchronization algorithms for grid-connected renewable energy systems: A review, Renewable & sustainable energy reviews, 2018, Vol. 90, pp. 434 – 452.

[33] Golestan S, Guerrero JM, Vasquez JC. Three-Phase PLLs: A Review of Recent Advances, IEEE transactions on power electronics, 2017, Vol. 32, Iss. (3), pp. 1894–1907.

[34] Luna A, Citro C, Gavriluta C, Hermoso J, Candela I, Rodriguez P. Advanced PLL structures for grid synchronization in distributed generation, Renewable Energy and Power Quality Journal, 2012, pp. 1747–1756.

[35] Luna A, Rocabert J, Candela I, Rodriguez P, Teodorescu R, Blaabjerg F. Advanced structures for grid synchronization of power converters in distributed generation applications, In: 2012 IEEE Energy Conversion Congress and Exposition (ECCE), IEEE, 2012, pp. 2769 – 2776.

[36] Guerrero-Rodríguez N., Rey-Boué AB, Rigas A, Kleftakis V. Review of Synchronization Algorithms used in Grid-Connected Renewable Agents. Renewable Energy and Power Quality Journal, 2014, pp. 240 – 245.

[37] Guerrero-Rodríguez N., Rey-Boué AB, Bueno E., Ortiz O, Reyes-Archundia E. Synchronization algorithms for grid-connected renewable systems: Overview, tests and comparative analysis, Renewable & sustainable energy reviews, 2017, Vol. 75, pp. 629 – 643.

[38] Jaalam N, Rahim N., Bakar AH., Tan C, Haidar AM. A comprehensive review of synchronization methods for grid-connected converters of renewable energy source, Renewable & sustainable energy reviews, 2016, Vol. 59, pp.1471 – 1481.

[39] Yu B. An improved frequency measurement method from the digital PLL structure for single-phase grid-connected PV applications. Electronics (Basel), 2018, Vol. 7, Iss. (8), p. 150.

[40] Khan S, Bletterie B, Anta A, Gawlik W. On small signal frequency stability under virtual inertia and the role of PLLs. Energies (Basel), 2018, Vol. 11, Iss. (9), p. 2372.

[41] Catherino HA, Feres FF, Trinidad F. Sulfation in lead–acid batteries. Journal of power sources, 2004, Vol. 129, Iss. (1), pp. 113 – 120.

[42] Karthigeyan V, Aswin M, Priyanka L, Sailesh KND, Palanisamy K. A comparative study of lithium ion (LFP) to lead acid (VRLA) battery for use in telecom power system. In: 2017 International Conference on Computation of Power, Energy Information and Commuincation (ICCPEIC), IEEE, 2017, pp. 742 – 748.

[43] Strzelecki RM. Power Electronics in Smart Electrical Energy Networks, 1st ed, London: Springer London, 2008, pp. 269 – 302.

[44] Divya K., Østergaard J. Battery energy storage technology for power systems—An overview, Electric power systems research, 2009, Vol. 79, Iss. (4), pp. 511 – 520.

[45] Eaton Corporation. Complete back up power made completely by Eaton, Product brochure, Eaton Supercapacitor back up power solution, Available: https://www.eaton.com/content/dam/eaton/products/backup-power-ups-surge-it-power-distribution/backup-power-ups/power-xpert-9395/eaton-supercapacitors-back-up-solution-brochure-br153059en.pdf (accessed Feb 2021).

[46] Eaton. Eatonin UPSG-konttiratkaisu, Website, Available: http://powerquality.eaton.com/suomi/products-services/backup-power-ups/upsg.asp?cx=79 (accessed Feb 2021).

[47] Basler M., Schaefer R. Understanding Power-System Stability. IEEE transactions on industry applications, 2008, Vol. 44, Iss. (2), pp. 463 – 474.

[48] Grigsby LL. Power system stability and control. 3rd ed. Boca Raton, Fla: CRC Press; 2012, pp. 116 – 127.

[49] Kundur P, Paserba J, Ajjarapu V, Andersson G, Bose A, Canizares C, et al. Definition and classification of power system stability IEEE/CIGRE joint task force on stability terms and definitions, IEEE transactions on power systems, 2004, Vol. 19, Iss. (3), pp. 1387 – 1401.

[50] Bevrani H. Robust Power System Frequency Control. 1st ed. 2009, New York, NY: Springer US, 2009.

[51] Obaid ZA, Cipcigan L., Muhssin MT. Fuzzy hierarchal approach-based optimal frequency control in the Great Britain power system, Electric power systems research, 2016, Vol. 141, pp. 529 – 537.

[52] Cosse RE, Alford MD, Hajiaghajani M, Hamilton ER. Turbine/generator governor droop/isochronous fundamentals - A graphical approach. In: 2011 Record of Conference Papers Industry Applications Society 58th Annual IEEE Petroleum and Chemical Industry Conference (PCIC), IEEE, 2011, pp. 1 – 8.

[53] Fingrid Oyj. Taajuuden vakautusreservien (FCR) teknisten vaatimusten todentaminen ja hyväksyttämisprosessi, Feb 2021 Available: https://www.fingrid.fi/globalassets/dokumentit/fi/sahkomarkkinat/reservit/fcr-liite2---teknisten-vaatimusten-todentaminen-ja-hyvaksyttamisprosessi.pdf (accessed Feb 2021).

[54] Fingrid Oyj. Fingrid Reservimarkkinat, Website, Available: https://www.fingrid.fi/sahkomarkkinat/reservit-ja-saatosahko/ (accessed Feb 2021).

[55] Fingrid Oyj. Nopean taajuusreservin (FFR) teknisten vaatimusten todentaminen ja hyväksyttämisprosessi, May 2020 Available: https://www.fingrid.fi/globalassets/dokumentit/fi/sahkomarkkinat/reservit/liite2---nopean-taajuusreservin-ffr-teknisten-vaatimusten-todentaminen-ja-hyvaksyttamisprosessi.pdf (accessed Feb 2021).

[56] Fingrid Oyj. Fingrid Nopea taajuusreservi, Website, Available: https://www.fingrid.fi/sahkomarkkinat/reservit-ja-saatosahko/nopea-taajuusreservi/ (accessed Feb 2021).

[57] ENTSO-E. Rate of Change of Frequency (RoCoF) withstand capability, ENTSO-E guidance document for national implementation for network codes on grid connection, Brussels, Belgium Nov 2017.

[58] Ponte P. Bulletin 5544421 Technical Information from Cummins, Transient Performance of Generating Sets, White Paper, Cummins Inc, USA Mar 2019.

[59] ISO 8528-5:2018 – Reciprocating internal combustion engine driven alternating current generating sets — Part 5: Generating sets, ISO standard, 4th Edition, Oct 2018.

[60] Mondal A, Renjit AA, Illindala MS, Eto JH. Operation and impact of energy storage system in an industrial microgrid. In: 2015 IEEE Industry Applications Society Annual Meeting, IEEE, 2015, pp. 1 – 7.

[61] Knap V, Sinha R, Swierczynski M, Stroe D-I, Chaudhary S. Grid inertial response with Lithium-ion battery energy storage systems. In: 2014 IEEE 23rd International Symposium on Industrial Electronics (ISIE), IEEE, 2014, pp. 1817 – 1822.

[62] Delille G, Francois B, Malarange G. Dynamic Frequency Control Support by Energy Storage to Reduce the Impact of Wind and Solar Generation on Isolated Power System's Inertia, IEEE transactions on sustainable energy, 2012, Vol. 3, Iss. (4), pp. 931 – 939.

[63] Mufti M ud din, Lone SA, Iqbal SJ, Ahmad M, Ismail M. Super-capacitor based energy storage system for improved load frequency control, Electric power systems research, 2009, Vol. 79, Iss. (1), pp. 226 – 233.

[64] Oudalov A, Chartouni D, Ohler C. Optimizing a Battery Energy Storage System for Primary Frequency Control, IEEE transactions on power systems, 2007, Vol. 22, Iss. (3), pp. 1259 – 1266.

[65] Alizadeh GA, Rahimi T, Nozadian MHB, Padmanaban S, Leonowicz Z. Improving microgrid frequency regulation based on the virtual inertia concept while considering communication system delay, Energies (Basel), 2019, Vol. 12, Iss. (10), p. 2016.

[66] Bevrani H, Ise T, Miura Y. Virtual synchronous generators: A survey and new perspectives, International journal of electrical power & energy systems, 2014, Vol. 54, pp. 244 – 254.

[67] Van de Vyver J, De Kooning JDM, Meersman B, Vandevelde L, Vandoorn TL. Droop Control as an Alternative Inertial Response Strategy for the Synthetic Inertia on Wind Turbines, IEEE transactions on power systems, 2016, Vol. 31, Iss. (2), pp. 1129 – 1138.

[68] Hesse R, Turschner D, Beck H-P. Micro grid stabilization using the virtual synchronous machine (VISMA), Renewable Energy and Power Quality Journal, 2009, Vol. 1, Iss. (7), pp. 676 – 681.

[69] Sakimoto K, Miura Y, Ise T. Stabilization of a power system with a distributed generator by a Virtual Synchronous Generator function. In: 8th International Conference on Power Electronics - ECCE Asia. Jeju, Korea (South), 2011, pp. 1498-1505.

[70] D'Arco S, Suul JA. Virtual synchronous machines - Classification of implementations and analysis of equivalence to droop controllers for microgrids. In: 2013 IEEE Grenoble Conference, IEEE, 2013. p. 1–7.

[71] Soni N, Doolla S, Chandorkar MC. Improvement of Transient Response in Microgrids Using Virtual Inertia. IEEE transactions on power delivery, 2013, Vol. 28, Iss. (3), pp. 1830 – 1838.

[72] Zhang T, Orr JA, Eigeles Emanuel A. Adaptable Energy Storage System Control for Microgrid Stability enhancement. In: 2018 IEEE Power & Energy Society General Meeting (PESGM), IEEE, 2018, p. 1 – 5.

[73] Masanet E, Shehabi A, Lei N, Smith S, Koomey J. Recalibrating global data center energy-use estimates. Science (American Association for the Advancement of Science), 2020, Vol. 367, Iss. (6481), pp. 984 – 986.

[74] Awasthi SR, Chalise S, Tonkoski R. Operation of datacenter as virtual power plant. In: 2015 IEEE Energy Conversion Congress and Exposition (ECCE), IEEE, 2015, pp. 3422 – 3429.

[75] Bajracharyay L, Awasthi S, Chalise S, Hansen TM, Tonkoski R. Economic analysis of a data center virtual power plant participating in demand response. In: 2016 IEEE Power and Energy Society General Meeting (PESGM), IEEE, 2016, pp. 1 – 5.

[76] IEEE Recommended Practice for Excitation System Models for Power System Stability Studies. IEEE Standard, Vol. 421, No. 5, 2016 (Revision of IEEE 521.5-2005).

[77] Mohsen S. Pilehvar, Behrooz Mirafzal. Frequency and Voltage Supports by Battery-Fed Smart Inverters in Mixed-Inertia Microgrids. Electronics (Basel), Oct 2020, Vol. 9, Iss. (1755), p. 1755.

[78] Eaton Corporation. Eaton 93PM UPS. Website, Available: https://www.eaton.com/us/en-us/catalog/backup-power-ups-surge-it-power-distribution/eaton-93pm-ups.html (accessed Feb 2021).

[79] AGCO Power. AGCO Power diesel generator AG250xA (250 kVA) Operator's Manual, 2019, p. 1.

APPENDIX A

Generating set parameters used in the simulations:

Parameter	1000 kVA Generator system[1]	250 kVA Generator system[2]
Rotor type	Salient-pole, 2 pole pairs	Salient-pole, 2 pole pairs
Nominal voltage (V)	400/230	400/230
Nominal Power (kVA)	1000	250
Nominal frequency (Hz)	50	50
Xd dir. axis synchronous (%)	2.73	1.37
X'd dir. axis transient (%)	0.22	0.09
X''d dir axis subtransient (%)	0.15	0.05
Xq quad. axis reactance (%)	1.61	0.78
X''q quad. axis subtransient (%)	0.19	0.15
XL leakage reactance	0.08	0.08
Rs stator resistance (Ω)	0.002	0.007
T'd transient time constant (s)	0.185	0.085
T''d subtransient time constant (s)	0.025	0.013
T'do open-circuit time constant (s)	3.03	1.3
Inertia constant H (s)[3]	0.28	0.12

1 *Based on Stamford HCI634J* **2** *Based on Mecc Alte ECO381L4A, some parameters are slightly adjusted* **3** *Calculated using* $H = WR^2 \cdot \frac{C}{S_{kVA}}$*, where* WR^2 *is rotor inertia in kgm², C is a constant that considers running speed and* S_{kVA} *is the kVA-rating of the generator.*